# Chapter 6

# A joint power-and-time allocation CSS scheme for energy harvesting multi-PUs, multi-SUs overlay CRNs

In today's tech-driven world, emerging technologies like the Internet of Things (IoT), Artificial Intelligence (AI), Cloud computing and digital communication are transforming the way we live, work, and communicate [46]. With the proliferation of these cutting-edge technologies, we are witnessing an unprecedented growth in the number of wireless devices. However, the smooth functioning of these devices depends heavily on the available spectrum resources in terms of bandwidth and/or access time and energy source associated with them. As the number of devices rapidly increases, researchers worldwide are facing significant challenges related to spectrum scarcity and energy constraints. Consequently, spectral efficiency and energy efficiency have emerged as critical design considerations in wireless communications [63]. Recent advancements in wireless technologies now allow for collecting energy and processing information from ambient radio frequency signals using wireless methods for information and power transfer. Cognitive radio offers a promising approach to improving spectrum utilization through spectrum sharing, addressing the ongoing resource shortage problem [8], [75]. Integrating cognitive radio technology with energy harvesting (EH) provides an efficient solution for energy-constrained devices (secondary users or SUs), enhancing both energy and spectrum utilization.

Traditionally, solar and wind power have been popular options for energy

harvesting. However, recent studies have uncovered the significant potential of radio-frequency (RF) signals for simultaneously carrying information and power, leading to the development of simultaneous wireless information and power transfer (SWIPT) technology [132], [67]. With suitable circuitry, a SWIPT receiver can effectively decode information and harvest energy from RF signals, extending the lifespan of wireless devices and the overall network. In SWIPT, receiver design can be categorized into three techniques: time switching (TS), power splitting (PS), and antenna switching (AS) [53]. TS and PS are the most commonly used approaches for wireless energy harvesting, while AS is considered a distinct case of the PS architecture [12], [76].

Most existing literature [132], [121], [119], [86], [50] focuses on either time switching (TS) or power splitting (PS) based SWIPT technologies independently (or separately) to optimize transmission time and power allocation for energy harvesting (EH) and information decoding (ID). To the best of our knowledge, few studies investigate both TS and PS based SWIPT technologies together, especially for energy-constrained SUs participating in cooperative communication with PUs. Furthermore, existing studies do not address optimizing the utility and operational duration of energy-constrained SUs in cognitive radio networks (CRNs). By simultaneously employing both time switching (TS) and power splitting (PS) techniques during the energy harvesting phase, SUs can accumulate more energy than using them separately. This contributes to extending the lifespan of the secondary network. Therefore, this research introduces a unified model that integrates TS and PS based SWIPT for energy harvesting in energy-constrained SUs within an overlay CRN. This model optimizes the allocation of harvested power to enhance the effectiveness of the secondary network. The primary contributions of this research are summarized as follows.

- We explore an energy harvesting overlay cognitive radio network, where energy-constrained SUs employ a joint Time Switching-Power Splitting SWIPT technology to extract energy from received PU signals. This is achieved through the optimal allocation of TS and PS factors.
- We determine the harvested power at the SUs from the harvested energy and strategically allocate this power to serve cooperative communication and secondary transmission purposes optimally.
- We introduce a cooperation strategy-based framework for cooperative communication among multiple PUs and SUs. This framework is designed based on the concept of many-to-one mapping to maximize both the individual

utility of SUs and the overall utility of the secondary network.

The rest of this chapter is organized as follows: Section 6.1 defines the problem, assumptions, and symbols and notations used. Section 6.2 discusses the system model. The proposed scheme is presented in Section 6.3. Section 6.5 covers simulation experiments and performance comparison analysis. Finally, Section 6.6 concludes the chapter.

## 6.1 Problem Statement

The problem is to develop an energy harvesting scheme for efficient cooperative communication among energy-constrained SUs and preferred PUs in a multi-PU, multi-SU overlay CRN scenario. The proposed scheme addresses three key objectives: (i) optimal allocation of TS-PS factors, (ii) optimal allocation of power allocation factors, and (iii) maximizing the efficacy of the secondary network. By formulating these as multi-objective optimization problems and using a heuristic solution approach based on numerical analysis, the proposed scheme aims to provide efficient solutions by integrating cooperative strategies among SUs.

### 6.1.1 Assumptions

- SUs use a time division sharing model based on TDMA for CSS over the PU band as described in [24].
- Transmission powers of PUs and SUs, distances between PUs and SUs, and other resource constraints of SUs are known.
- SUs are energy-constrained nodes and adopt an energy-harvesting data-transmission mode.
- Each SU is equipped with rechargeable batteries with some initial energy (negligible) and uses non-linear energy harvesters to gather energy from RF signal [93].
- The maximum battery capacity for storing harvested energy is known to each SU. The target decoding rate constraint of PUs and the target transmission constraint of SUs are known.
- The locations of SUs and PUs are fixed; they remain stationary during energy harvesting and the partner assignment process.

- All SUs in the network are non-malicious, and their resource information is trustworthy.
- All SUs willingly adopt a cooperative strategy to increase individual and cooperative profit.
- The noise environment is assumed to be zero-mean Additive White Gaussian Noise (AWGN), and the channel gain between nodes depends only on distance and path loss components [100], [97].
- Necessary control information exchange between PU and SU takes place through a dedicated common control channel [80] These control information focuses on the operational aspects of communication to ensure efficient channel usage.

### 6.1.2 Notations and Symbols Used

To remind the symbols and notations used particularly in this chapter, the same are summarized in Table 6.1.

| Symbols/Notations | Comments |
|---|---|
| $\mathcal{M}$ | Set of PUs |
| $\mathcal{N}$ | Set of SUs |
| $M$ | Number of PUs |
| $N$ | Number of SUs |
| $F$ | Number of frames in a PU band |
| $W$ | Total bandwidth of PU channel |
| $T$ | Total access time of each frame of PU band |
| $d_{PT,PR}$ | Euclidean Distance between PT and PR (in m) |
| $d_{PT,ST}$ | Euclidean Distance between PT and ST (in m) |
| $d_{ST,PR}$ | Euclidean Distance between ST and PR (in m) |
| $d_{ST,SR}$ | Euclidean Distance between ST and SR (in m) |
| $P_{PT}$ | Transmission power of PU |
| $U_{PU}$ | Utility achieved by PU |
| $U_{SU}$ | Utility achieved by SU |
| $\alpha$ | Time allocation factor |
| $\rho$ | Power splitting factor |
| $\eta$ | Energy conversion efficiency |
| $x$, $y$ | Power allocation factors |

| | |
|---|---|
| $\omega$ | Negligible value |
| $\pi$ | Partition of SUs |
| $R_{PT}^{tar}$ | Targeted transmission rate of PU |
| $R_{ST}^{tar}$ | Targeted transmission rate of SU |
| $EH_{T_1}^{max}$ | Maximum possible energy harvesting at ST during $T_1$ duration |
| $R_{T_1}^{max}$ | Maximum possible decoding rate at ST during $T_1$ duration |
| $EH_{T_1}^{prop}$ | Achieved harvested energy at ST during $T_1$ duration in proposed scheme. |
| $R_{T_1}^{prop}$ | Achieved decoding rate at ST during $T_1$ duration in proposed scheme. |
| $HP_{ST}^{prop}$ | Achieved harvested power at ST in proposed scheme. |
| $R_{T_2}^{prop}$ | Instantaneous achievable rate at PR during $T_2$ duration in proposed scheme. |
| $C_{PT}^{coop}$ | Cooperative capacity achieved by PT during $T_1 + T_2$ duration in proposed scheme. |
| $R_{T_3}^{prop}$ | Instantaneous achievable rate at SR during $T_3$ duration in proposed scheme. |
| $TP_{ST}^{ava}$ | Total power available at ST after energy harvesting. |
| $OU_{SN}$ | Overall utility of secondary network. |
| $SAT_{ST}$ | Avg. satisfaction of SUs |
| $\%P_{ST}$ | Percentage of SUs participated in coop. communication |

Table 6.1: Notations and Symbols used

## 6.2 System Model

We consider a Cognitive Radio Network (CRN) framework which consists of a set of $M$ primary user (PU) transceiver pairs, denoted as $\mathcal{M} = \{PT_i, PR_i\}_{i=1}^{M}$, and $N$ secondary user (SU) transceiver pairs ($|M| < |N|$), denoted as $\mathcal{N} = \{ST_j, SR_j\}_{j=1}^{N}$. This configuration is shown in Figure 6-1. Each primary transceiver ($PT_i$) aims to transmit data to its dedicated primary receiver ($PR_i$)

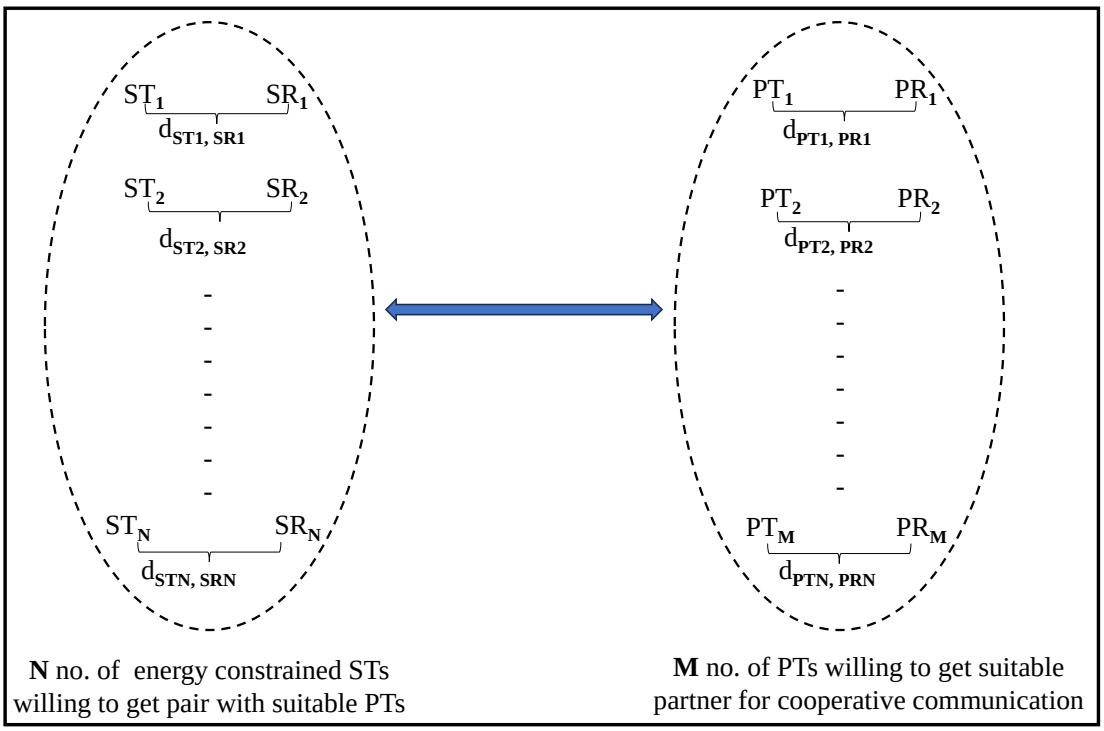


**Figure 6-1:** Considered PU-SU scenario for energy efficient cooperative communication

over a predefined number of transmission frames. However, if the transmission range between $PT$ and $PR$ (denoted as $d_{PT,PR}$) exceeds the effective communication range, an ST, acting as a relay node, is required to forward information from $PT$ to $PR$ to achieve a minimum targeted transmission rate ($R_{PT}^{tar}$). In exchange for this assistance, STs gain spectrum access opportunities over the PU band using an overlay access paradigm [34], [79], [103] for secondary communication towards secondary receivers ($SR$). It is essential to note that the STs are energy-constrained nodes operating in an energy-harvesting data-transmission mode. These STs have a minimum required transmission rate, $R_{ST}^{tar}$, which must be met. Moreover, STs are equipped with rechargeable batteries and utilize non-linear energy harvesters to extract energy from the primary signals they receive [93], [31]. It is assumed that rechargeable batteries have a finite energy capacity, $BE_{finite}$ with a negligible initial energy, $BE_0$. All nodes within this network operate in half-duplex mode, each equipped with a single antenna.

In our proposed approach, we adopt a frame-based information transmission system between the PT and PR using TDMA. The time division structure of each frame within a PU band is illustrated in Figure 6-2. A PU band comprises $F$ transmission frames, each lasting $T$ sec. Each frame is subdivided into three sub-slots: $T_1$, $T_2$, and $T_3$ respectively. During the $T_1$ sub-slot (Phase 1), PT transmits its signal to the ST. Within this time, the ST performs two critical

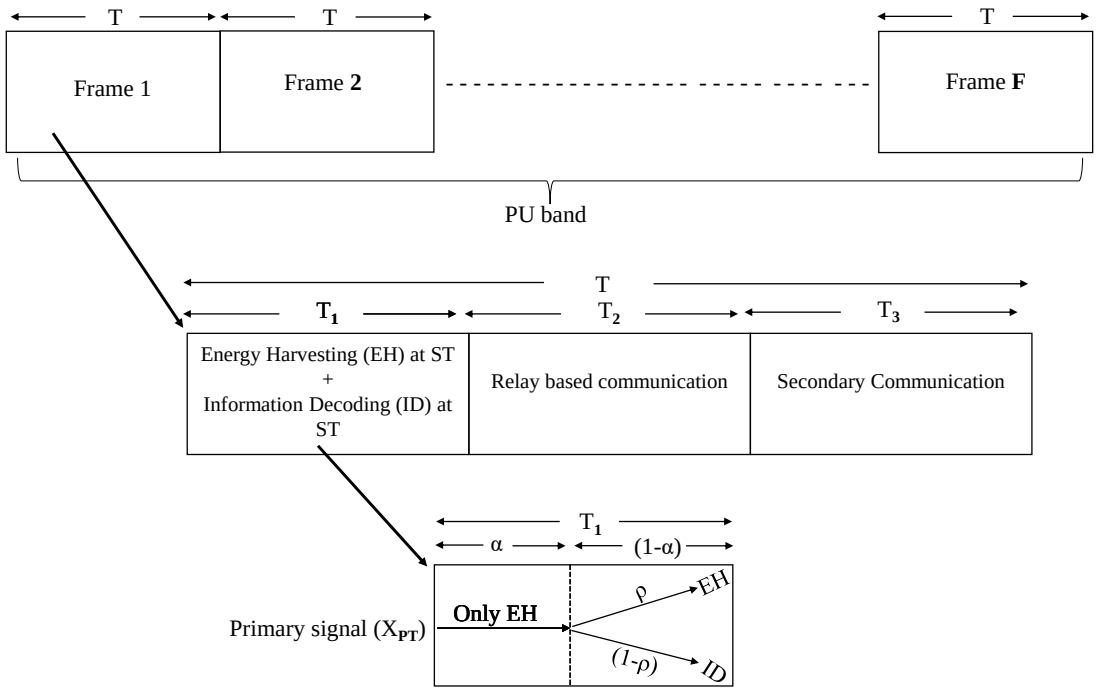


**Figure 6-2:** Frame-wise time-slot division structure of a PU band for EH and ID

tasks: it harvests energy from the received primary signal and decodes the primary information for subsequent processing. In the $T_2$ sub-slot (Phase 2), the ST utilizes a portion of the harvested energy to forward the primary signal to the PR using a Decode and Forward (DF) relaying technique. Finally, in the $T_3$ sub-slot (Phase 3), the ST engages in secondary transmission, utilizing the remaining harvested energy for its own data transmission. This structured approach ensures efficient utilization of time and resources within the PU band for both primary and secondary communication processes. The following paragraphs outline the three phases involved in energy harvesting and cooperative communication:

### Phase 1: Energy Harvesting and Information Decoding by ST

When $PT$ transmits its information to $ST$, the received signal at $ST$ can be expressed as given in Eq.(6.1).

$$Y^I_{PT,ST} = \sqrt{P_{PT}} h_{PT,ST} X^I_{PT} + N_{0,a} + N_{0,cov} \tag{6.1}$$

Here, $P_{PT}$ represents the transmit power of the $PT$, $h_{PT,ST}$ signifies the channel gain between $PT$ and $ST$, $X^I_{PT}$ corresponds to the transmitted signal from $PT$ intended for $PR$, $N_{0,a} \sim \mathcal{CN}(0, \sigma^2_{N_{0,a}})$ represents the narrow band Gaus-

sian noise generated by the antenna at $ST$ and $N_{0,cov} \sim \mathcal{CN}(0, \sigma^2_{N_{0,cov}})$ denotes the RF-to-baseband signal conversion noise at $ST$. Further, $h_{PT,ST}$ is defined as channel gain between PT and ST with path loss component 2. The received signal undergoes both energy harvesting and information decoding, which is based on the Dynamic Power Splitting (DPS) technique. In this regard, we draw inspiration from [132] and [119], to model the maximum achievable harvested energy ($EH^{max}_{T_1}$) at $ST$, in Joules, during the $T_1$ time interval. The modeling equation for $EH^{max}_{T_1}$ is presented in Eq.(6.2).

$$EH^{max}_{T_1} = T_1 \eta P_{PT} \left|h_{PT,ST}\right|^2 \tag{6.2}$$

Here, $\eta$ represents the energy conversion efficiency ($0 < \eta < 1$) at $ST$.

On the other hand, the maximum achievable instantaneous decoding rate ($R^{max}_{T_1}$), at $ST$ (in bps), during $T_1$ time is given by Eq.(6.3).

$$\begin{aligned} R^{max}_{T_1} &= WT_1 \log_2\left(1 + SNR_{PT,ST}\right) \\ &= \left(WT_1 \log_2\left(1 + \frac{P_{PT}\left|h_{PT,ST}\right|^2}{\sigma^2_{N_{0,a}} + \sigma^2_{N_{0,cov}}}\right)\right) \end{aligned} \tag{6.3}$$

Utilizing the principles of simultaneous wireless information and power transfer (SWIPT) and DPS, our proposal introduces a unified TS-PS technique. This technique enables the simultaneous extraction of energy and information from the primary signal received. As illustrated in Figure 6-2, we divide the time slot $T_1$ into two sub-slots, guided by a TS parameter denoted as $\alpha$ (where $0 < \alpha < 1$). During the $\alpha T_1$ duration, the entire received power from the primary signal is dedicated to energy harvesting. Conversely, in the remaining $(1-\alpha)T_1$ duration, the signal power dynamically partitions into two distinct power streams, establishing a power ratio of $\rho$ : (1-$\rho$). Here, $\rho$ (where $0 < \rho < 1$) is allocated to energy harvesting, while (1-$\rho$) is allocated to the primary signal decoding at the ST. To provide clarity and a comprehensive understanding, we express the mathematical formulation of $\rho$ for both time intervals, $\alpha T_1$ and $(1-\alpha)T_1$, as outlined in Eq. (6.4) and Eq. (6.5), respectively.

$$\rho_{\alpha T_1} = \begin{cases} 1, & \text{for EH} \\ 0, & \text{for ID} \end{cases} \tag{6.4}$$

$$\rho_{(1-\alpha)T_1} = \begin{cases} \rho, & \text{for EH} \\ (1-\rho), & \text{for ID} \end{cases} \tag{6.5}$$

By substituting the expressions from Eq. (6.4) and Eq. (6.5) into Eq. (6.2), we can reformulate the harvested energy for our proposed approach, denoted as $EH_{ST}^{prop}$, as presented in Eq. (6.6).

$$\begin{aligned} EH_{ST}^{prop} &= \Big(\alpha T_1 \eta P_{PT} \left|h_{PT,ST}\right|^2\Big) + \Big((1-\alpha) T_1 \eta \rho P_{PT} \left|h_{PT,ST}\right|^2\Big) \\ &= \Big(\Big(\alpha + (1-\alpha)\rho\Big) T_1 \eta P_{PT} \left|h_{PT,ST}\right|^2\Big) \end{aligned} \tag{6.6}$$

Similarly, by substituting the expressions from Eq. (6.4) and Eq. (6.5) into Eq. (6.3), we can reformulate the achievable instantaneous decoding rate during Phase 1 for our proposed approach, denoted as $R_{T_1}^{prop}$, as represented in Eq. (6.7).

$$\begin{aligned} R_{T_1}^{prop} &= W T_1 \log_2(1 + SNR_{PT,ST}) \\ &= \left(W(1-\alpha) T_1 \log_2\Big(1 + \frac{(1-\rho) P_{PT} \left|h_{PT,ST}\right|^2}{(1-\rho)\sigma_{N_{0,a}}^2 + \sigma_{N_{0,cov}}^2}\Big)\right) \end{aligned} \tag{6.7}$$

Taking inspiration from [93] and [31], we consider a non-linear energy harvesting receiver. Using this receiver, we formulate the total harvested power at $ST$ for our proposed work, denoted as $HP_{ST}^{prop}$, as demonstrated in Eq. (6.8).

$$HP_{ST}^{prop} = \begin{cases} \frac{\eta(1+\rho) P_{PT} |h_{PT,ST}|^2}{(1-\alpha)}, & \text{for} \quad P_{PT}|h_{PT,ST}|^2 \leq P_{th} \\ \frac{\eta(1+\rho) P_{th}}{(1-\alpha)}, & \text{for} \quad P_{PT}|h_{PT,ST}|^2 > P_{th} \end{cases} \tag{6.8}$$

Here, we define $P_{th}$ as the saturation threshold power of the energy har-

vesting circuit at $ST$. Towards the end of this phase, we calculate the total power available at $ST$, denoted as $TP_{ST}^{ava}$, according to the formulation presented in Eq. (6.9).

$$TP_{ST}^{ava} = HP_{ST}^{prop} + P_{ST}^{min} \tag{6.9}$$

Here, $P_{ST}^{min}$ represents the minimum required power for an $ST$ to remain active in the network.

**Phase 2: Cooperative Communication by ST**

During this phase, $ST$ forwards a portion of the received signal, specifically $(1-\rho)Y_{PT,ST}^{I}$, to $PR$ using the available total power $TP_{ST}^{ava}$. However, it's important to note that $ST$ also has responsibilities for secondary communication in Phase 3. To accommodate these dual tasks, a fraction of the total power, denoted as $xTP_{ST}^{ava}$, is allocated for relaying the primary signal in Phase 2, while another fraction, $yTP_{ST}^{ava}$, is reserved for secondary communication in Phase 3. It's important to emphasize that both $x$ and $y$ are constrained to the range $0 < x, y < 1$. Consequently, as Phase 2 concludes, we can express the received primary signal at $PR$ using the formulation provided in Eq. (6.10).

$$\begin{aligned} Y_{ST,PR}^{II} &= \sqrt{xTP_{ST}^{ava}} h_{ST,PR}(1-\rho)Y_{PT,ST}^{I} + N_{0,awgn} \\ &= \left( \sqrt{xTP_{ST}^{ava}} h_{ST,PR} \Big( \sqrt{(1-\rho)P_{PT}} h_{PT,ST} X_{PT}^{I} + N_{0,a} + N_{0,cov} \Big) + N_{0,awgn} \right) \end{aligned} \tag{6.10}$$

Here, $N_{0,awgn}$ is the additive White Gaussian Noise (AWGN) at $PR$. At this juncture, we can express the received Signal-to-Noise Ratio ($SNR$) at $PR$ as presented in Eq. (6.11).

$$SNR_{ST,PR} = \frac{xTP_{ST}^{ava} \left| h_{ST,PR} \right|^2}{x\sigma_{N_{0,a}}^2 + \sigma_{N_{0,cov}}^2} \tag{6.11}$$

Likewise, we can reformulate the instantaneous achievable rate at $PR$ during Phase 2 for our proposed approach, denoted as $R_{T_2}^{prop}$, using the equation

provided in Eq. (6.12).

$$R_{T_2}^{prop} = WT_2 \log_2(1 + SNR_{ST,PR}) \tag{6.12}$$

At this point, we can analyze the cooperative capacity ($C_{PT}^{coop}$) achieved by PT, leveraging DF relaying assistance from $ST$ over Phases 1 and 2. Drawing from insights in [108], we can model the resulting $C_{PT}^{coop}$ over a bandwidth $B$ and a total time duration of $T_1 + T_2$ using the Shannon-Hartley theorem [70]. The equation representing this model is provided as Eq. (6.13).

$$C_{PT}^{coop} = \Big(W\big(T_1 + T_2\big) log_2\big(1 + SNR_{PT,ST} + SNR_{ST,PR}\big)\Big) \tag{6.13}$$

**Phase 3: Secondary Communication by ST**

In the final phase, $ST$ engages in secondary communication by transmitting its own signal towards $SR$, utilizing a power allocation of $yTP_{ST}^{ava}$. As a result, we can formulate the received $SNR$ at $SR$ using the equation provided in Eq. (6.14).

$$SNR_{ST,SR} = \frac{yTP_{ST}^{ava} \left|h_{ST,SR}\right|^2}{x\sigma_{N_{0,a}}^2 + \sigma_{N_{0,cov}}^2} \tag{6.14}$$

Similarly, we can reformulate the instantaneous achievable rate at $SR$ during Phase 3 for our proposed approach, denoted as $R_{T_3}^{prop}$, as presented in Eq. (6.15).

$$R_{T_3}^{prop} = WT_3 \log_2(1 + SNR_{ST,SR}) \tag{6.15}$$

## 6.3 Problem Formulation

### 6.3.1 Performance metrics

In our study of the proposed energy-harvesting Cognitive Radio Network model, we investigated two distinct theoretical metrics to assess its performance. The first metric, known as the Rate-Energy (R-E) Tradeoff, involves the optimization of the time-switching factor $\alpha$ and power splitting ratio $\rho$. This optimization aims to strike a balance between the energy harvested by the $ST$ and the maintenance of the primary information decoding rate at $ST$. The second metric we consider is the system utility of SUs ($U_{SU}$), which serves as a measure of the secondary network's efficiency. This metric quantifies efficiency in terms of the bps/Joule metric.

- *(i) R-E Tradeoff:* Given the energy constraints faced by SUs, there's a significant inclination for the $ST$ to prioritize energy harvesting from the received primary signal. Consequently, the $ST$ tends to allocate a substantial portion of the received signal power for energy harvesting. However, it simultaneously must uphold $R_{T_1}^{prop}$ to meet the requirements of $R_{PT}^{tar}$. This presents a tradeoff scenario where balancing the maximization of $EH_{ST}^{prop}$ and maintaining $R_{T_1}^{prop}$ is essential. Drawing inspiration from [132] and [119], we introduce the term R-E region ($RE_{reg}^{prop}$) to characterize these tradeoffs among $EH_{ST}^{prop}$ and $R_{T_1}^{prop}$ based on the decision variables $\alpha$ and $\rho$. The model for this R-E region is as follows:

$$RE_{reg}^{prop} = \bigcup_{\alpha,\rho} \left\{ \begin{array}{l} (EH, R): \\ EH_{ST}^{prop} \leq EH_{ST}^{max}, \\ R_{PT}^{tar} < R_{T_1}^{prop} < R_{T_1}^{max} \end{array} \right\}$$

- *(ii) System Utility of SUs*: With the decision variables $x$ and $y$ at play, the primary goal of $ST$ is to maximize the instantaneous achievable rate during secondary transmission while minimizing its total energy consumption. To quantify this, we model $U_{SU}$ as a fraction of the achievable transmission rate by $ST$ during Phase 3 in relation to the total energy consumption (EC) by $ST$ over both Phase 2 and Phase 3. This model is expressed as given in Eq.

(6.16):

$$U_{SU} = \frac{R_{T_3}^{prop}}{\underbrace{xTP_{ST}^{ava}}_{\text{EC in Phase 2}} + \underbrace{yTP_{ST}^{ava}}_{\text{EC in Phase 3}}} \tag{6.16}$$

### 6.3.2 Formulation of Optimization Problems

In our study, we address two optimization problems. The first problem aims to maximize energy harvesting at $ST$ during Phase 1. In this problem, we seek to determine the optimal values for (i) the time-switching factor $\alpha$ and (ii) the power-splitting factor $\rho$. The second problem focuses on maximizing the system utility of SUs during Phase 3. Here, we aim to find the optimal values for (iii) $x$ and $y$, which represent the total power allocation factors for SUs during Phase 2 and 3, respectively.

1. **Optimization Problem 1 (OP1)**
   The primary objective of OP1 is to maximize energy harvesting from the received primary signal while ensuring the successful decoding of primary information. This is achieved through the optimal allocation of $\alpha$ and $\rho$. The formulation of OP1 is presented below:

$$\begin{aligned} \textbf{OP1:} \quad \arg\max_{\alpha,\rho} \quad & EH_{ST}^{prop} \\ \text{s.t.} \quad & (a) 0 < \alpha < 1 \\ & (b) 0 < \rho < 1 \\ & (c) R_{PT}^{tar} \leq R_{T_1}^{prop} \\ & (d) EH_{ST}^{prop} \leq EH_{ST}^{max} \\ & (e) EH_{ST}^{prop} < BE_{finite} \end{aligned} \tag{6.17}$$

2. **Optimization Problem 2 (OP2)**
   The primary objective of OP2 is to maximize the system utility of SUs ($U_{sys}^{prop}$) through optimal allocation of $x$ and $y$. This allocation aims to ensure that both the primary transmission rate constraint during Phase 2 and the secondary transmission rate constraint during Phase 3 are met. Here, $(1-(x+y))TP_{ST}^{ava}$ is the remaining power at ST (denoted as $P_{ST}^{r}$) after completion of both cooperative and secondary transmission. The formulation of OP2 is

presented below:

$$\begin{aligned} \textbf{OP2:} \quad \arg\max_{x,y} \quad & U_{sys}^{prop} \\ \text{s.t.} \quad & (a) 0 < x < 1 \\ & (b) 0 < y < 1 \\ & (c)(1-(x+y))TP_{ST}^{ava} \leq P_{ST}^{min} \\ & (d) R_{PT}^{tar} \leq R_{T_2}^{prop} \\ & (e) R_{ST}^{tar} < R_{T_3}^{prop} \end{aligned} \tag{6.18}$$

### 6.3.3 Nature of Optimization Problems

Both optimization problems, denoted as OP1 and OP2, are characterized by their non-linear nature. In OP1 and OP2, the mathematical expressions involve mixed polynomials, and the interdependencies among the decision variables $\alpha$, $\rho$, $x$, and $y$ exhibit non-linearity. Specifically, $\alpha$ is subject to multiplication by $\rho$, while $x$ undergoes both multiplication and division by $y$. Additionally, it is essential to note that each of these decision variables is constrained to fall within the rational range of (0, 1). This constraint stipulates that the optimal values for $\alpha$, $\rho$, $x$, and $y$ must be rational numbers. Theoretical insights from prior research, specifically Theorems 1 and 2 in a related study [42] and Theorem 2.1 in another study [28], have demonstrated that solving non-linear problems characterized by mixed polynomial equations with rational coefficients falls within the NP-hard category, making them computationally intractable. Inspired by the findings of references [42] and [28], it can be concluded that the proposed optimization problems, as represented by Eq. (6.17) and Eq. (6.18), also belong to the class of NP-hard problems. The non-linear and NP-hard nature of these optimization problems necessitates the utilization of advanced optimization techniques to efficiently obtain approximate or near-optimal solutions. In the existing literature, techniques such as Approximation algorithms and Heuristic algorithms have been widely employed to tackle similar challenging problems. Consequently, we have developed numerical analysis-based quick iterative heuristic solutions, outlined in Algorithm 8 (for OP1) and Algorithm 9 (for OP2), aimed at obtaining near-optimal solutions for the decision variables $\alpha$, $\rho$, $x$, and $y$.

**Algorithm 8:** In Algorithm 8, we initially limit the values of $\alpha$ and $\rho$ to the interval (0, 1). To simplify the initial setup, we select the midpoint of this interval

as the starting value for the parameter $\rho$. This choice ensures an equal distribution of power between energy harvesting (EH) and information decoding (ID) over the time $(1-\alpha)T_1$. As the number of iterations for determining $\rho^*$ and $\alpha^*$ increases, the range (0, 1) progressively narrows down towards the optimal values of $\alpha^*$ and $\rho^*$. Simultaneously, the initial value of $\rho$ adjusts itself towards $\rho^*$ by either increasing or decreasing in steps of $\Delta\rho$. The algorithm continues this search operation until the difference between the two search values in the shrinking range approaches zero (or becomes negligible, say $\omega$). At this point, we can achieve the maximum $EH_{ST}^{prop}$ that satisfies $R_{PT}^{prop}$.

**Time Complexity of Algorithm 8:** To analyze the overall time complexity of Algorithm 8, we shall begin by examining the running time of the ***inner for loop*** (step 2). Let us consider that the initial length of the range $\alpha$ = (0,1), is equal to $n$. During each iteration of the inner loop, $n$ is halved, and this process continues until $\frac{n}{2}$ is less than or equal to $\omega$. Assuming the inner loop runs for a maximum of $k$ times, we can express this as $\frac{n}{2^k} \leq \omega$, which leads to $k = O(Nlog\frac{n}{\omega})$. Given that we consider $N$ SUs, the inner for loop runs $O(Nlog\frac{n}{\omega})$ times. Now, for a total of $M$ PUs, the outer for loop (step 1) runs $M$ times. Consequently, the overall running time of Algorithm 1 can be characterized as $O(MNlog\frac{n}{\omega})$, which represents a ***polynomial time*** complexity.

**Proof of Continuity:** To prove the continuity of the proposed objective function (Eq. (6.17)), with respect to the decision variable $\alpha \in (0, 1)$ and $\rho \in (0, 1)$, the concept of differentiability is applied. Since differentiability implies continuity, demonstrating that the objective function is differentiable in $\alpha$ and $\rho$ within the said interval will automatically establish its continuity in the same interval. Let's analyze the proof.

- Simplifying and cancelling the constant terms of the objective function, Eq. (6.17), the simplified form in terms of $\alpha$ and $\rho$ is written as:

$$f(\alpha, \rho) = (\alpha + (1 - \alpha)\rho)C^3 \tag{6.19}$$

- To check differentiability, we need to verify if the derivatives of $f(\alpha, \rho)$ with respect to $\alpha$ and $\rho$ exist for all $\alpha, \rho \in (0, 1)$. For this, lets first calculate $f'_\alpha(\alpha, \rho)$ as follows:

**Algorithm 8:** Computation of $\alpha^*$ and $\rho^*$ for energy harvesting in Phase 1 .

**Input:** $R_{PT}^{tar}$, $T_1$, $W$, $P_{PT}$, $\eta$ of $M$ PU's and $EH_{ST}^{max}$, $h_{PT,ST}$, $\Delta\rho$ of $N$ SUs, $\omega$.
**Output:** $\alpha^*$, $\rho^*$ computed by each SU for each PU band.

**for** *each PU band* **do**
  **for** *each SU* **do**
    **Initialize** low = 0 and high = 1, $\rho = 0.5$ and $\rho_{new} = \rho$.
    Calculate $\alpha_m = \frac{low+high}{2}$, $\alpha_{m-1} = \frac{low+\alpha_m}{2}$, $\alpha_{m+1} = \frac{\alpha_m+high}{2}$ //where, $\alpha_m, \alpha_{m-1}, \alpha_{m+1} \in (0,1)$
    Calculate $EH$ and $R$ for $\alpha_m$, $\alpha_{m-1}$, $\alpha_{m+1}$, and $\rho_{new}$ points, based on Eq. (6.6) and Eq. (6.7).
    **if** ($EH_{\alpha_{m+1}} < EH_{ST}^{max}$ && $E_{\alpha_{m+1}} > E_{\alpha_m}$ && $E_{\alpha_{m+1}} > E_{\alpha_{m-1}}$ && $R_{\alpha_{m+1}} > R_{PT}^{tar}$) **then**
      low = $\alpha_{m+1}$, high = high.
      **REPEAT** steps 4 and 5.
      $\rho_{new} = \frac{\rho_{new}+(\rho_{new}+\Delta\rho)}{2}$
    **else if** ($EH_{\alpha_{m+1}} < EH_{ST}^{max}$ && $E_{\alpha_{m+1}} > E_{\alpha_m}$ && $E_{\alpha_{m+1}} > E_{\alpha_{m-1}}$ && $R_{\alpha_{m+1}} < R_{PT}^{tar}$) **then**
      low = $\alpha_m$, high = $\alpha_{m+1}$.
      **REPEAT** steps 4 and 5.
      $\rho_{new} = \frac{\rho_{new}+(\rho_{new}-\Delta\rho)}{2}$
      **Continue** till ($R_{\alpha_{m+1}} > R_{PT}^{tar}$)
    **else if** ($EH_{\alpha_m} < EH_{ST}^{max}$ && $E_{\alpha_m} > E_{\alpha_{m-1}}$ && $R_{\alpha_m} > R_{PT}^{tar}$) **then**
      low = $\alpha_m$, high = $\alpha_{m+1}$.
      **REPEAT** steps 5 and 6.
      $\rho_{new} = \frac{\rho_{new}+(\rho_{new}+\Delta\rho)}{2}$
    **else if** ($EH_{\alpha_m} < EH_{ST}^{max}$ && $E_{\alpha_m} > E_{\alpha_{m-1}}$ && $R_{\alpha_m} < R_{PT}^{tar}$) **then**
      low = $\alpha_{m-1}$, high = $\alpha_m$.
      **REPEAT** steps 4 and 5.
      $\rho_{new} = \frac{\rho_{new}+(\rho_{new}-\Delta\rho)}{2}$
      **Continue** till ($R_{\alpha_m} > R_{PT}^{tar}$)
    **else if** ($EH_{\alpha_{m-1}} < EH_{ST}^{max}$ && $R_{\alpha_{m-1}} > R_{PT}^{tar}$) **then**
      low = $\alpha_{m-1}$, high = $\alpha_m$.
      **REPEAT** steps 4 and 5.
      $\rho_{new} = \frac{\rho_{new}+(\rho_{new}+\Delta\rho)}{2}$
    **else if** ($EH_{\alpha_{m-1}} < EH_{ST}^{max}$ && $R_{\alpha_{m-1}} < R_{PT}^{tar}$) **then**
      low = low, high = $\alpha_m$.
      **REPEAT** steps 4 and 5.
      $\rho_{new} = \frac{\rho_{new}+(\rho_{new}-\Delta\rho)}{2}$
      **Continue** till ($R_{\alpha_{m-1}} > R_{PT}^{tar}$)
    **end**
    **if** ($|\alpha_m - \alpha_{m-1}| \leq \sigma$) && ($|\alpha_{m+1} - \alpha_m| \leq \omega$) **then**
      Identify Max($EH_{\alpha_{m-1}}$, $EH_{\alpha_m}$, $EH_{\alpha_{m+1}}$) and Max($R_{\alpha_{m-1}}$, $R_{\alpha_m}$, $R_{\alpha_{m+1}}$).
      Find $\alpha$ and $\rho$ from the results obtained in step 36 and marked them as $\alpha^*$ and $\rho^*$.
    **else**
      **GO TO** step 5 and **Repeat** till step 34.
    **end**
  **end**
  Based on the computed $\alpha^*$ and $\rho^*$, each SU calculates Max. possible $EH_{ST}^{prop}$ for each PU band.
**end**

$$f'_{\alpha}(\alpha,\rho) = \frac{d}{d\alpha}\left((\alpha+(1-\alpha)\rho)C^3\right) = C^3(1-\rho) \tag{6.20}$$

Similarly calculate $f'_{\rho}(\alpha,\rho)$ as follows:

$$f'_{\rho}(\alpha,\rho) = C^3(1-a) \tag{6.21}$$

- To check the existence of the derivative, let verify the following points :
  - Both the derivatives $f'_{\alpha}(\alpha,\rho)$ and $f'_{\rho}(\alpha,\rho)$ are linear functions in $\alpha$ and $\rho$.
  - Both the derivatives are continuous in domain $(0,1)\times(0,1)$.

  Thus, $f(\alpha,\rho)$ is differentiable and differentiability implies continuity, we conclude that $f(\alpha,\rho)$ is continuous in the specified ranges $\alpha \in (0,1)$ and $\rho \in (0,1)$.

### 6.3.4 Performance analysis with Optimal results

Utilizing Algorithm 8, we have depicted the achieved $EH_{ST}^{prop}$ resulting from the optimal allocation of $\alpha^*$ and $\rho^*$ in Figure 6-3 (other simulation parameters are listed in Table 3). This approach attains an impressive accuracy of 97.7% when compared to the optimal (benchmark) result obtain from lingo optimization tool [3]. It is noteworthy that when considering individual values of $\alpha^*$ and $\rho^*$, the proposed solution still demonstrates strong correctness, with accuracy rates of 96% and 95%, respectively, when compared to the benchmark values of $\alpha^*$ and $\rho^*$. These findings underscore the effectiveness and reliability of our proposed solution technique in approximating near-optimal allocation points for $\alpha$ and $\rho$, ultimately leading to significant improvements in the energy harvesting capability of ST.

We then explored the influence of the distance between $PT$ and $ST$ while optimizing the allocation of $\alpha^*$ and $\rho^*$ for EH. The results of this investigation are presented in Figure 6-4. When $ST$ (the relay) is in close proximity to $PT$, the value of $h_{PT,ST}$ is notably favorable. This proximity enhances the strength of $PT's$ signal power at $ST$. Consequently, by allocating a small fraction of $\alpha = 0.1258$ during the $\alpha T_1$ time slot, $ST$ can reach its maximum possible harvested energy level, which is 35 Joules. In this juncture, it's important to note that during

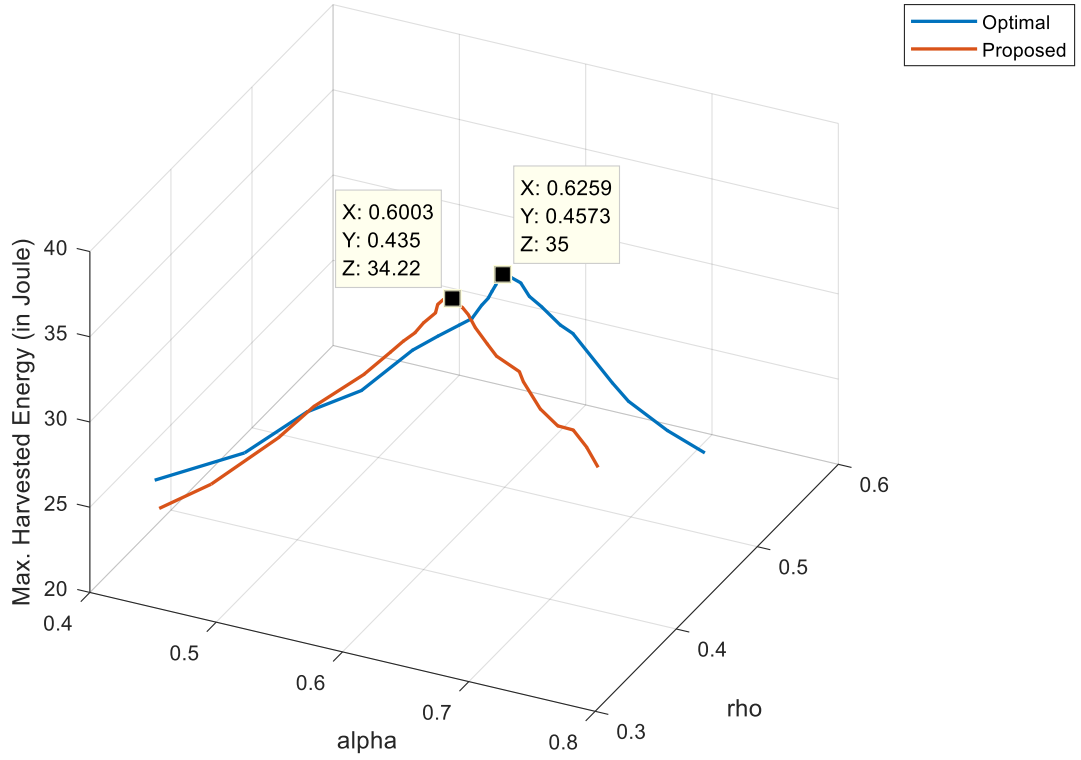


**Figure 6-3:** Max. harvested energy vs. optimal allocation of $\alpha^*$ and $\rho^*$

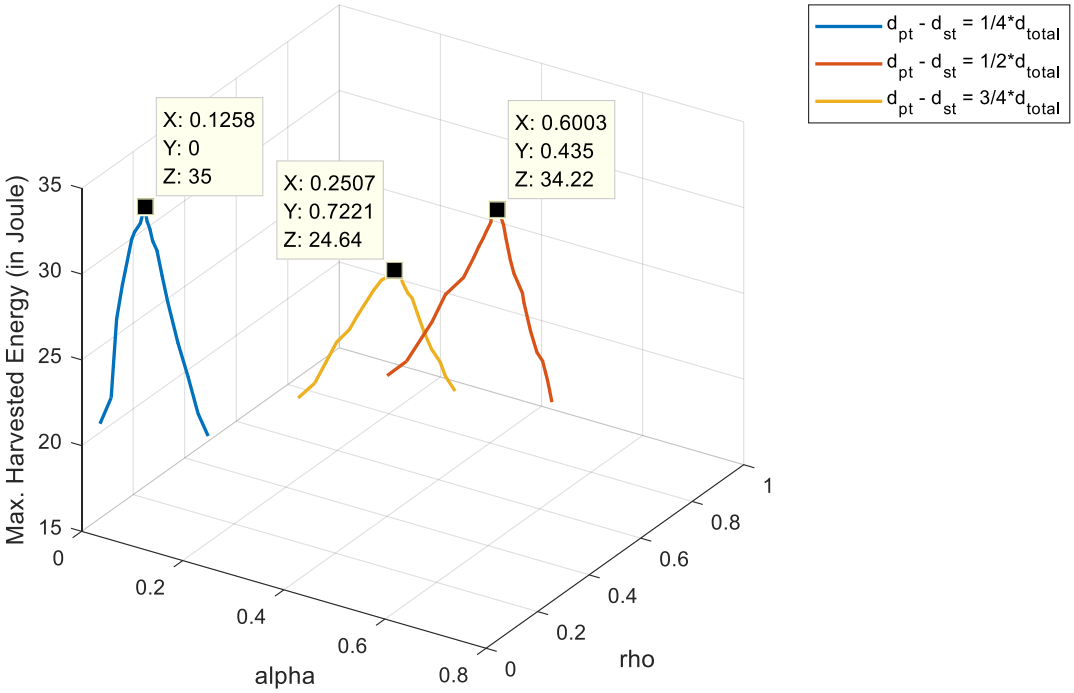


**Figure 6-4:** Max. harvested energy vs. optimal allocation of $\alpha^*$ and $\rho^*$ for varying distances between $PT$ and $ST$

the remaining $(1-\alpha)T_1$ time, all signal power is solely dedicated to information decoding, implying that $\rho = 0$

Conversely, when $ST$ is situated farther away from $PT$, the quality of the channel ($h_{PT,ST}$) between them degrades, resulting in a limited amount of energy available for harvesting by $ST$. In such scenarios, $ST$ tends to allocate a larger portion of signal power for energy harvesting during the $(1-\alpha)T_1$ time slot, while still satisfying the decoding rate constraint of $PT$. For instance, by allocating $\alpha = 0.2507$ for $\alpha T_1$ time, a substantial fraction of $\rho = 0.7221$ can be allocated for $(1-\alpha)T_1$ time. This allocation allows $ST$ to harvest approximately 24.64 Joules of energy over the $T_1$ time duration. When $ST$ is positioned at an intermediate distance between $PT$ and $PR$, a balanced approach can be taken. In this case, by allocating $\alpha = 0.6003$ and $\rho = 0.435$, as discussed in Figure 6-4, $ST$ can harvest a total of 34.22 Joules of energy.

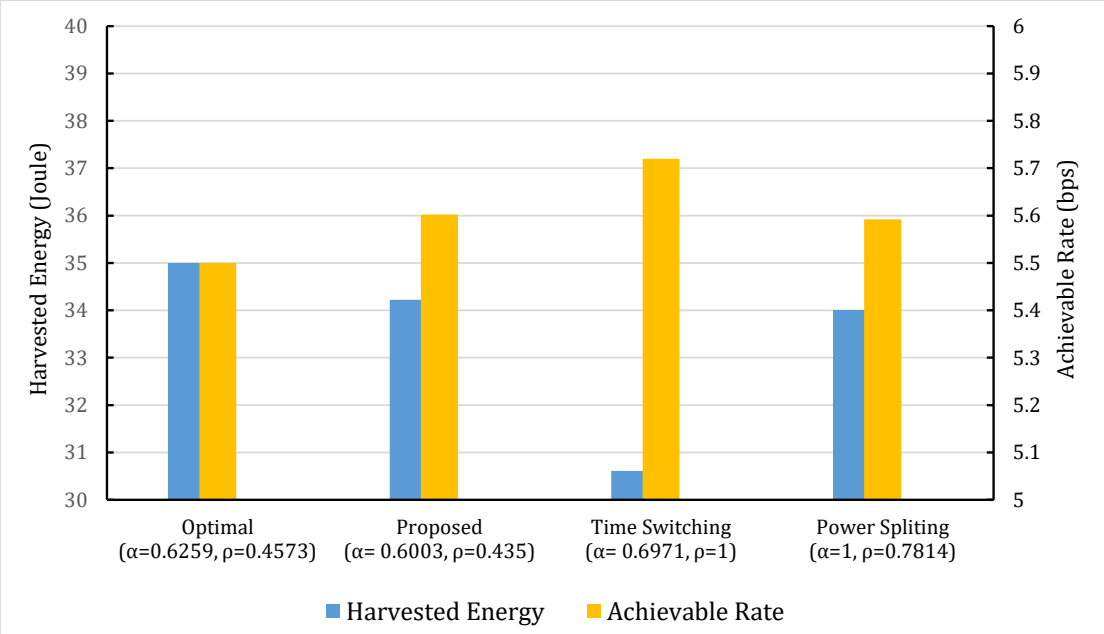


**Figure 6-5:** Performance analysis of harvested energy vs. achievable rate among different approaches

In Figure 6-5, we compare the graph depicting the achieved harvested energy versus the instantaneous decoding rate for the proposed technique with two other existing techniques in [132] and [93]. In the time switching technique [132], all signal power (i.e., $\rho = 1$) is allocated for energy harvesting during the $\alpha T_1$ time slot, and in the subsequent $(1-\alpha)T_1$ time slot, all signal power is dedicated to information decoding. On the other hand, in the power splitting technique discussed in [93], the total signal power is divided into two streams with the power ratio $\rho : (1-\rho)$ for energy harvesting and information decoding, respectively. Observ-

ing the graph, we note that, apart from the optimal configuration, the proposed technique outperforms both the time switching and power splitting techniques. This improvement is achieved through the proper allocation of $\alpha$ and $\rho$, which not only increases the harvested energy at $ST$ but also ensures the satisfaction of the decoding rate constraint (5.5 bps) for $PT$. It's worth mentioning that in the case of the power splitting technique [93], the performance of both EH and ID is found to be approximately 99% accurate when compared to the proposed technique.

**Algorithm 9** Algorithm 9 operates with the primary input being $TP_{ST}^{ava}$, which is obtained by converting the harvested energy, as determined by Algorithm 8 (as per Eq. (6.8) and Eq.(6.9)). The main objective of Algorithm 9 is to optimize the allocation of $TP_{ST}^{ava}$ for Phases 2 and 3 by determining the values of $x^*$ and $y^*$. In this process, we begin with the initial range for both $x$ and $y$ set as $[0, 1]$. The central concept behind this proposed strategy revolves around dynamically partitioning the given range of $(0, 1)$ into two sub-ranges for $x$ and $y$. As the sub-range for $x$ narrows towards the left (i.e., towards 0) in the pursuit of finding $x^*$, the sub-range for $y$ simultaneously expands in search of $y^*$ that maximizes $U_{SU}$. These iterations persist until the difference between the search values of $x$ and $y$ ranges approaches nearly zero or becomes negligible, while achieving the maximum possible $U_{SU}$.

**Time Complexity of Algorithm 9:** To analyze the overall time complexity of Algorithm 9, let us begin by examining the running time of the inner for loop (step 2). Consider that $x$ and $y$ are in the range $(0, ..., i, ..., 1)$, and the length of this range, denoted as $(0, ..., i, ..., 1)$, is represented by $n$. We can individually express $x$ as $(0, i)$ and $y$ as $(i + 1, 1)$. The length of $(0, i)$ is $n_1$, and the length of $(i + 1, 1)$ is $n_2$, where $n = n_1 + n_2$. During each iteration of both $x$ and $y$, $n_1$ and $n_2$ are reduced by half and continue until $\frac{n_1}{2} \leq \omega$ and $\frac{n_2}{2} \leq \omega$. Assuming that the iterations in $x$ run a maximum of $k_1$ times, we can express this as $\frac{n_1}{2^{k_1}} \leq \omega$, which implies $k_1 = O(\log \frac{n_1}{\omega})$. Similarly, if the iterations in $y$ run a maximum of $k_2$ times, we can express it as $k_2 = O(\log \frac{n_2}{\omega})$. Now, when we combine these values, we can express $k = k_1 + k_2 = O(\log \frac{n_1+n_2}{\omega}) = O(\log \frac{n}{\omega})$. Since there are a total of $N$ SUs, the inner for loop runs $O(N \log \frac{n}{\omega})$ times. For a total of $M$ PUs, the outer for loop (step 1) runs $M$ times. Consequently, the overall running time of Algorithm 2 is $O(MN \log \frac{n}{\omega})$, which signifies a polynomial time complexity.

**Algorithm 9:** Computation of $x^*$ and $y^*$ for Power Allocation in Phase 2 and 3.

**Input:** $R_{PT}^{tar}$, $T_2$, $T_3$, $W$ of $M$ PUs and $TP_{ST}^{ava}$, $P_{ST}^{min}$, $R_{ST}^{tar}$, $h_{ST,PR}$, $h_{ST,SR}$ of $N$ SUs, $\omega$.

**Output:** $x^*$, $y^*$ computed by each SU for each PU band.

**for** *each PU band* **do**
  **for** *each SU* **do**
    **Initialize** low = 0, high = 1.
    Calculate $x_m = \frac{low+high}{2}$, $x_{m-1} = \frac{low+x_m}{2}$, $x_{m+1} = \frac{x_m+high}{2}$ //where, $x_m, x_{m-1}, x_{m+1} \in (0,1)$
    Calculate $RT2$ for $x_{m-1}$, $x_m$ and $x_{m+1}$ points, based on Eq. (6.12).
    **if** *($RT2_{x_{m-1}} > R_{PT}^{tar}$)* **then**
      $x_{low}$= low, $x_{high} = x_{m-1}$ and $y_{low} = x_{high}$, $y_{high} = 1 - x_{high}$.
      Calculate $x_m = \frac{x_{low}+x_{high}}{2}$, $x_{m-1} = \frac{x_{low}+x_m}{2}$, $x_{m+1} = \frac{x_m+x_{high}}{2}$.
      Calculate $y_m = \frac{y_{low}+y_{high}}{2}$, $y_{m-1} = \frac{y_{low}+y_m}{2}$, $y_{m+1} = \frac{y_m+y_{high}}{2}$ //where, $y_m, y_{m-1}, y_{m+1} \in (0,1)$
    **else if** *($RT2_{x_m} > R_{pt}^{tar}$)* **then**
      $x_{low} = x_{m-1}$, $x_{high} = x_m$ and $y_{low} = x_{high}$, $y_{high} = 1 - x_{high}$.
      **REPEAT** steps 8 and 9.
    **else if** *($RT2_{x_{m+1}} > R_{pt}^{tar}$)* **then**
      $x_{low} = x_m$, $x_{high} = x_{m+1}$ and $y_{low} = x_{high}$, $y_{high} = 1 - x_{high}$.
      Repeat steps 8 and 9.
    **end**
    Calculate $RT2$, $RT3$ for $x_{m+1}$ and $y_{m-1}$ points, based on Eq.(6.12) and Eq.(6.15).
    Calculate $U$, $P^r$ for $x_{m+1}$, $y_{m-1}$ points based on Eq.(6.16), Eq.(6.18) and store in an array.
    **if** *($RT2_{x_{m+1}} > R_{PT}^{tar}$ && $RT3_{y_{m-1}} > R_{ST}^{tar}$ )* **then**
      $x_{low} = x_{low}$, $x_{high} = x_{m+1}$ and $y_{low} = x_{high}$, $y_{high} = y_{high}$.
      **REPEAT** steps 8, 9 and 18.
      Compare current and previous stored $U$ and $P^r$ values from the array.
      **if** *(current $U$ and $P^r$ > previous $U$ and $P^r$)* **then**
        **CONTINUE** from step 20 to 22.
      **else**
        $x_{low}$=$x_{m+1}$ (obtained for current $U$ value stored in the array).
        $x_{high}$=$x_{m+1}$ (obtained for previous $U$ value stored in the array).
        $y_{high}$=$y_{low}$ and $y_{low}$=$x_{high}$.
        **REPEAT** steps 8 and 9.
        **if** *(difference between $x_{m+1}$ and $y_{m-1}$ is $\leq \omega$ )* **then**
          **STOP** and termed the current $x_{m+1}$ as $x^*$ and $y_{m-1}$ as $y^*$.
        **else**
          **REPEAT** step 18.
          **REPEAT** step 23.
        **end**
      **end**
    **else**
      $x_{low} = x_{m+1}$, $x_{high} = x_{high}$ and $y_{low} = x_{high}$, $y_{high} = y_{high}$.
      **GO TO** step 21 and **REPEAT**.
    **end**
    **end**
  **end**
  Each SU computes $x^*$, $y^*$ for each PU band and accordingly allocates power for Phase 2 and 3.
**end**

**Proof of Continuity:** To prove the continuity of the proposed objective function (Eq. (6.18)), with respect to the decision variable $x \in (0,1)$ and $y \in (0,1)$, we will use the concept of differentiability. Since differentiability implies continuity, demonstrating that the objective function is differentiable in $x$ and $y$ within the said interval will automatically establish its continuity in the same interval. Let's analyze the proof.

- Simplifying and cancelling the constant terms of the objective function, Eq. (6.17), the simplified form in terms of $\alpha$ and $\rho$ is written as:

$$f(x,y) = \frac{C\log\left(1+\frac{yC^2}{xC+C}\right)}{C(x+y)} = \frac{\log\left(1+\frac{yC}{x+1}\right)}{x+y} \tag{6.22}$$

- To check differentiability, we need to verify if the derivative of $f(x,y)$ exists for all $x \in (0,1)$ and for all $y \in (0,1)$. For this, lets first calculate $f'_x(x,y)$ as follows:

$$f'_x(x,y) = \frac{\left(C\cdot\frac{-yC^3}{(xC+C)^2(1+\frac{yC^2}{xC+C})}\right)(xC+yC) - C\log\left(1+\frac{yC^2}{xC+C}\right)C}{(xC+yC)^2} \tag{6.23}$$

  Similarly, calculate $f'_y(x,y)$ as follows:

$$f'_y(x,y) = \frac{\left(C\cdot\frac{C^2}{(xC+C)(1+\frac{yC^2}{xC+C})}\right)(xC+yC) - C\log\left(1+\frac{yC^2}{xC+C}\right)C}{(xC+yC)^2} \tag{6.24}$$

- To check the existence of the derivative, let verify the following points :
  - In both the derivatives, the term $\frac{yC^2}{xC+C}$ is positive and continuous for $x, y \in (0,1)$.
  - The term $(xC+yC)$ is continuous in domain $(0,1)\times(0,1)$.
  - the logarithmic term $log(1+\frac{yC^2}{xC+C})$ is also positive and continuous for $x, y \in (0,1)$.

  Since, $f'_x(x,y)$ and $f'_y(x,y)$ involve continuous functions divided by non-zero continuous functions (denominator does not vanish), then the derivatives $f'_x(x,y)$ and $f'_y(x,y)$ are said to be continuous within the domain $(0,1)\times(0,1)$. Thus, $f(x,y)$ is differentiable and differentiability implies continuity, which implies $f(x,y)$ is continuous in the specified range $x \in (0,1)$ and $y \in (0,1)$.

### 6.3.5 Performance analysis with Optimal results

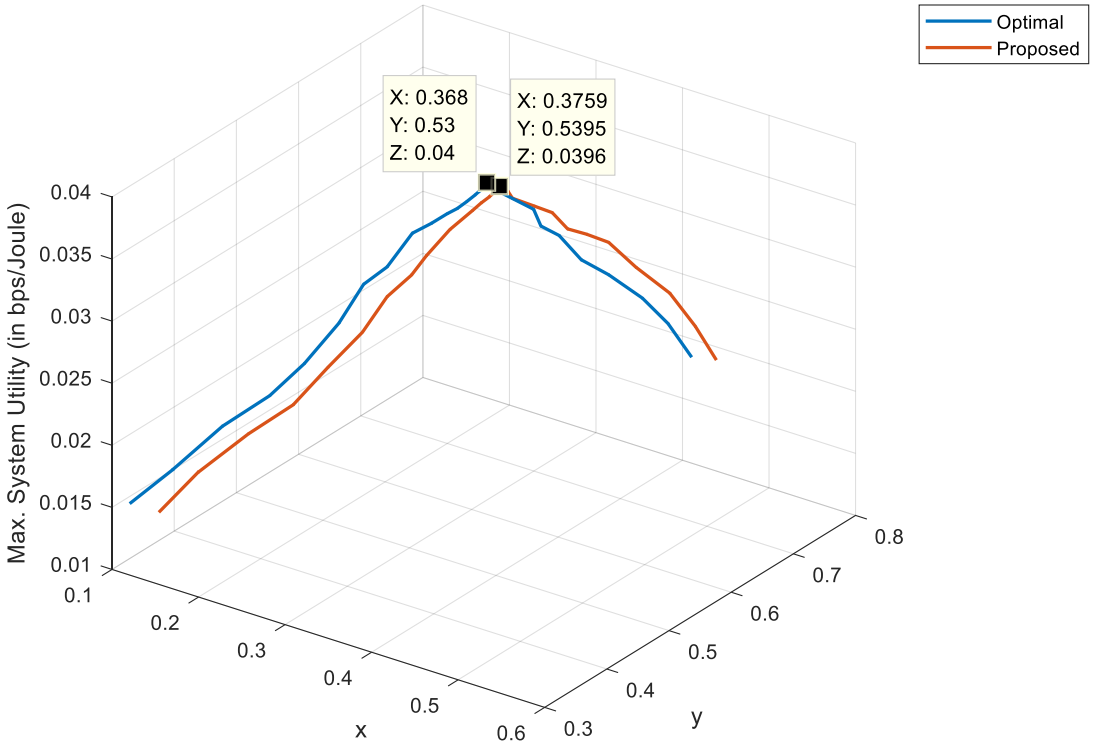


**Figure 6-6:** Max. system utility vs. optimal allocation of $x^*$ and $y^*$

In Figure 6-6, we present the graph of $U_{SU}$ derived using Algorithm 9, with appropriate allocations of $x^*$ and $y^*$. This graph serves as a basis for comparing the performance with the optimal (benchmark) result obtain from lingo optimization tool [3]. Notably, the attained $U_{SU}$ demonstrates an impressive level of accuracy, reaching 98.5%. Specifically, when we consider the allocation of $x^*$ and $y^*$ using the proposed technique, we observe correctness levels of 97.8% and 98% in comparison to the optimal result. This highlights the robustness and effectiveness of the proposed approach in achieving high levels of accuracy in system performance evaluation.

We now turn our attention to investigating the influence of the distance between $ST$ and $PR$ on the allocation of $x^*$ and $y^*$ for optimizing System Utility. The results of this investigation are visually presented in Figure 6-7. When $ST$ is in close proximity to $PR$, the $h_{ST,PR}$ value indicates strong signal strength between them, signifying favorable conditions. Consequently, by allocating a small fraction of the total power ($x = 0.0715$) in Phase 2, we can achieve the desired $R_{PT}^{prop}$, enabling $ST$ to allocate a larger fraction of total power ($y = 0.53$) in Phase 3. This strategic allocation results in the maximum attainable $U_{SU} = 0.05986$.

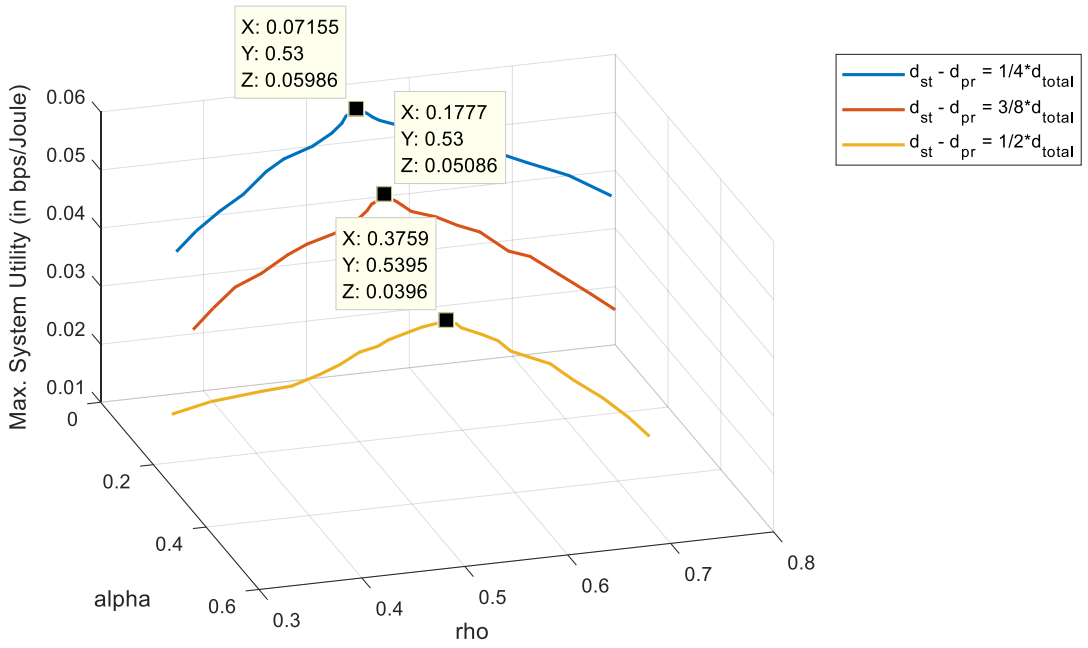


**Figure 6-7:** Max. system utility vs. optimal allocation of $x^*$ and $y^*$ for varying distances between $ST$ and $PR$

However, as the distance between $ST$ and $PR$ gradually increases, the quality of $h_{ST,PR}$ begins to degrade. Consequently, to meet the target $R_{PT}^{tar}$, $ST$ must invest more power in Phase 2 by increasing the value of $x$, as illustrated by the red and yellow graphs in Figure 6-7. This increased allocation of power during Phase 2, while effective in maintaining the desired rate, comes at the cost of higher energy consumption for $ST$, which in turn reduces the achievable $U_{SU}$, as visually depicted in the figure.

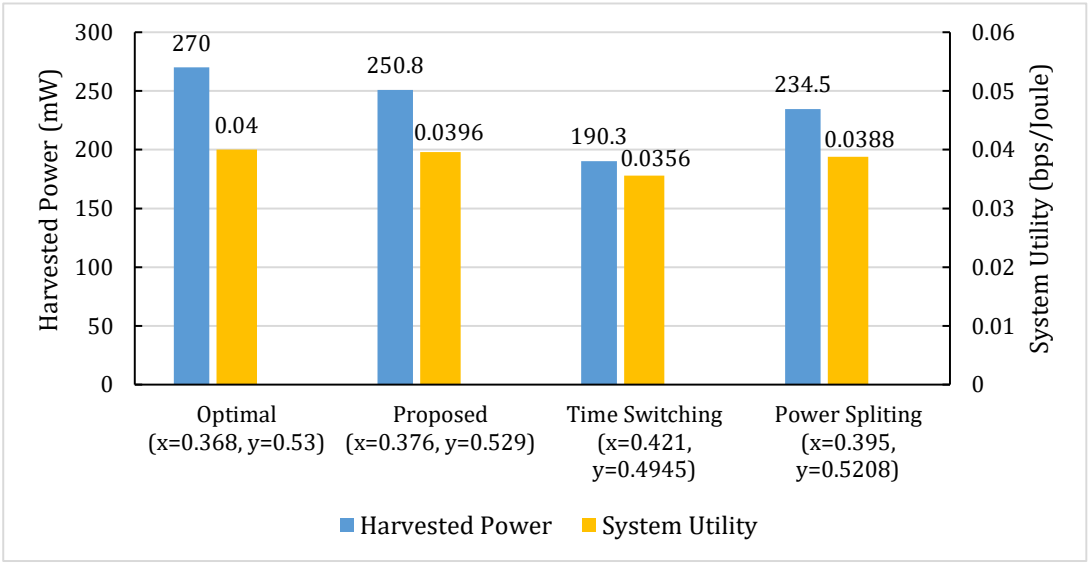


**Figure 6-8:** Performance analysis of achievable system utility vs. harvested power among different approaches

Finally, in Figure 6-8, we compare the graph depicting the Max. $U_{SU}$ versus the harvested power ($HP_{ST}^{prop}$) achieved at ST for the proposed technique with the existing techniques [132] and [93]. The $HP_{ST}^{prop}$ for the work [132] is calculated by reformulating Eq. (6.8) based on time switching (TS) technique as described in the work [132]. Similarly, $HP_{ST}^{prop}$ for the work [93] is calculated by reformulating Eq. (6.8) based on the Eq. (6) given in [93]. Observing the graph, we note that, apart from the optimal configuration, the proposed technique outperforms both the TS technique in [132] and PS technique in [93] in terms of maximum system utility and harvested power. This improvement is achieved due to the large power harvested by the ST in proposed technique than the TS and PS techniques discussed in [132] and [93] respectively. This helps the ST to allocate a large fraction of $HP_{ST}^{prop}$ ($y = 0.5395$) for secondary communication, which ultimately enhance $U_{SU}$ of ST than the discussed TS and PS techniques as depicted in the graph.

A comparison analysis among the proposed algorithms (Algorithm 8 for allocation of $\alpha^*$, $\rho^*$ and Algorithm 9 for allocation of $x^*$, $y^*$) and existing algorithms as discussed in [132] and [93] is conducted as shown in Table 6.2. It is noted that the values of relevant parameters used during simulations are derived from the information presented in Table 6.3 in section 6.5.

| **Parameters** | **Optimal** | **Proposed** | **PS** [93] | **TS** [132] |
|---|---|---|---|---|
| $\alpha^*$ | 0.6259 | 0.6003 | 1 | 0.6971 |
| $\rho^*$ | 0.4573 | 0.4350 | 0.6971 | 1 |
| Max. energy harvesting at SU (Joule) | 35 | 34.22 | 30.608 | 34.007 |
| Max. information decoding rate (bps) | 5.5 | 5.602 | 5.59 | 5.72 |
| $x^*$ | 0.368 | 0.3759 | 0.3946 | 0.4207 |
| $y^*$ | 0.53 | 0.5295 | 0.4941 | 0.4945 |
| Max. harvested power at SU (mW) | 270 | 250.8 | 234.5 | 190.3 |
| Max. system Utility of SU (bps/Joule) | 0.040 | 0.0396 | 0.0388 | 0.0356 |

Table 6.2: Comparison analysis with existing methods

## 6.4 Proposed cooperative communication framework for PUs and SUs

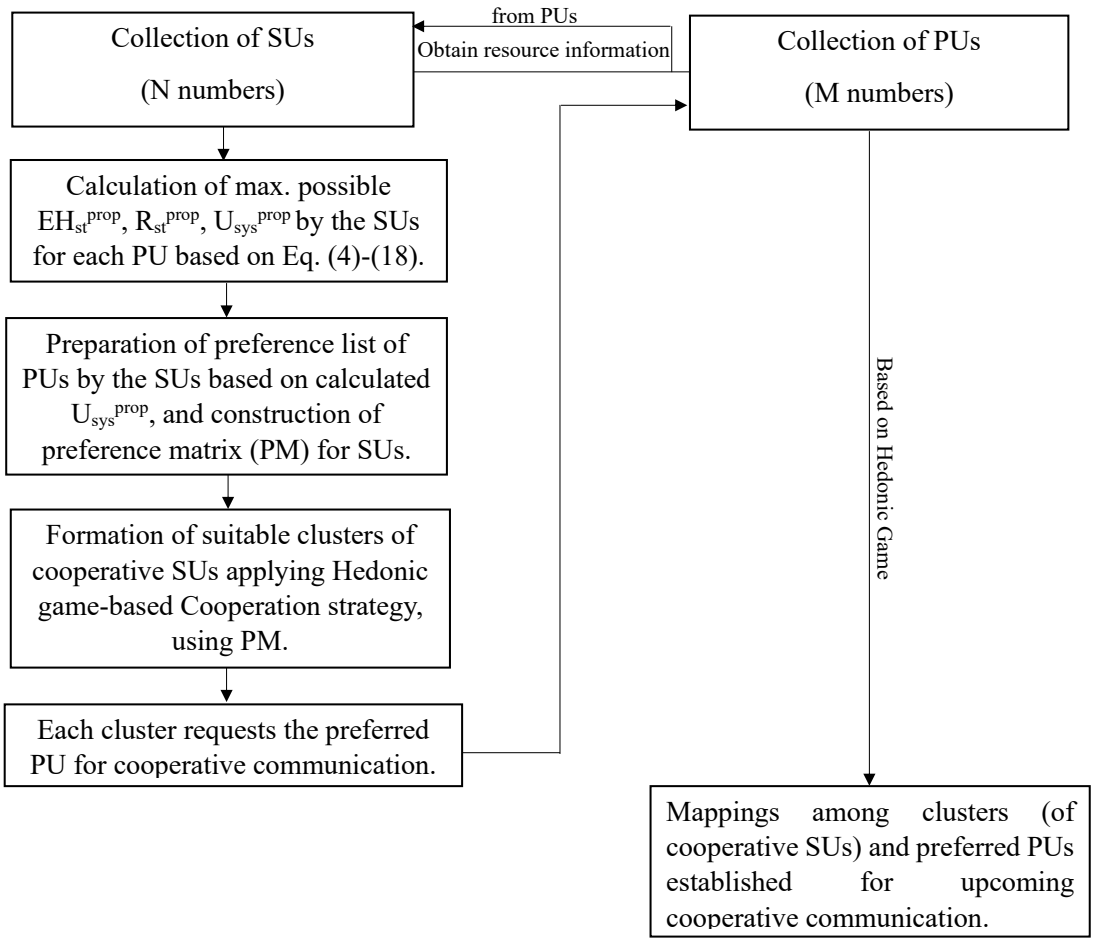


**Figure 6-9:** Block diagram for proposed cooperative communication framework

In pursuit of elevating the performance of the secondary network, energy-constrained secondary users (SUs) are keen on establishing partnerships with their most preferred primary users (PUs). Their objective is twofold: to harvest the maximum possible energy and to optimize the overall system utility during cooperative communication. To achieve this goal, a cooperation strategy has been devised and embraced by the SUs, intending to establish a many-to-one mapping between cooperative SUs and their favored PU. This strategy involves grouping SUs with shared PU preferences, enabling them to collectively access the PU spectrum for secondary transmission. The basic block diagram for the proposed cooperative communication among PUs and SUs is depicted in Figure 6-9.

In this section, we delve into the intricacies of this proposed cooperation strategy implemented by the SUs. We also explore the dynamics of cooperative communication among PUs and SUs, which ultimately lead to the emergence

of gross (or group) utility among cooperative SUs, denoted as $GU_{SU}$ and the overall utility of the secondary network, denoted as $OU_{SN}$. The formulation geared towards attaining the maximum achievable $OU_{SN}$ is modelled as follows:

$$\begin{aligned} OU_{SN} &= \arg\max_{C \subset C'} \left( \sum_{q=1}^{|C|} GU_{SU_{C_q}} \right) \\ &= \arg\max_{C \subset C'} \left( \sum_{q=1}^{|C|} \sum_{k=1}^{|K|} U_{SU_{q,k}} \right) \end{aligned} \tag{6.25}$$

Here, $C'$ represents all possible combinations of clusters comprising cooperative SUs, while $C$ denotes the total count of clusters or coalition formed through the proposed technique, with the constraint that $|C| \leq |M|$. Additionally, we denote $K$ is the total number of SUs in each cluster. It's important to emphasize that, for the entire duration of the cooperation process, we assume that all SUs are inherently trustworthy and dependable. To facilitate the formation of these clusters of SUs, we employ a Hedonic coalition formation game [15, 16, 33]. This game serves the purpose of grouping SUs in a manner that aligns with their preferences for cooperative communication with specific PUs. In essence, it strategically maps clusters of SUs to their preferred PUs, fostering effective cooperation within the network.

### 6.4.1 Hedonic coalition formation game

To establish many-to-one mapping among cooperative SUs and preferred PUs, we consider a Hedonic coalition formation game (HG) [33], [21], defined as a pair $(N, PM)$, where $N$ represents the set of secondary users (SUs), and PM stands for the preferences matrix that captures the preferences of SUs regarding each primary user (PU) in the network. This preference matrix has dimensions $[N \times M]$, where $N$ is the number of SUs and $M$ is the number of available PUs. Within this framework, we aim to establish a partition of SUs, denoted as $\pi$, where $\pi$ consists of disjoint clusters with a total of $C$ clusters, expressed as $\pi = \sum_{q=1}^{|C|} c_q$. The formation of this partition $\pi$ in a Hedonic coalition formation game involves the following principles:

- Individually Rational (IR): For the partition $\pi$ to be considered IR, it should

ensure that no single SU has an incentive to remain isolated without being part of any cluster $c_q \in C$ [15, 39].

- Nash Stable (NS): A partition $\pi$ is said to be NS when no SU can improve its situation by moving from its current coalition to another coalition (which could even be an empty one) [19], [20].
- Core Stable (CS): In the context of $\pi$, a coalition $c_b$ is deemed a blocking coalition if any SU within it strictly prefers the coalition $c_b$ over their current coalition $c_q$. A partition $\pi$ is considered CS, when it does not allow the existence of such blocking coalitions [16, 21].

These principles guide the formation of coalitions in the Hedonic coalition formation game, ensuring that the resulting partition satisfies criteria related to individual rationality, stability, and the absence of blocking coalitions. Drawing from the principles outlined in the HG concept discussed above, we introduce Algorithm 10. The primary objective of Algorithm 10 is to effectively divide the set of N SUs into C distinct and favorable clusters. This partitioning process is designed to achieve three essential properties, namely (i) *Individually Rational*: that is no SU is incentivized to remain isolated without belonging to any cluster; (ii) *Nash Stable*: This means that once the partition is established, no SU can improve its position by switching to another coalition, even if that coalition happens to be empty, and (iii) *Core Stable*: In the context of the partition formed, there should be no coalition (or group of SUs) that can block the formation, indicating that each SU in a cluster prefers to stay in their current coalition over any other. Moreover, Algorithm 10 seeks to associate each SU within a cluster with their preferred PU for the purpose of cooperative communication. This strategic alignment enhances both the individual group utility within each cluster and the overall utility of the entire set of SUs, $N$. The ultimate goal is to maximize the utility of the entire secondary network while ensuring that each SU is placed in an advantageous coalition with their preferred PU.

**Algorithm 10** Algorithm 10 takes as its primary inputs the $N$ SUs and their corresponding $U_{SU}$ values obtained through Algorithm 9 for each PU. Leveraging this information, each SU constructs a preference list (PL) of PUs by arranging the $U_{SU}$ values in descending order. This process results in the creation of an $N \times M$ preference matrix of PUs. The core objective of Algorithm 10 is to organize the $N$ SUs into appropriate clusters. This arrangement is designed to ensure that each secondary transmitter ($ST_j$) belonging to a cluster ($c_q$) is paired

**Algorithm 10:** Cluster formation and cooperative communication among SUs and preferred PU.

**Input:** $M$ PUs and $N$ SUs with associated resource information.
**Output:** Partition of $N$ SUs into $C$ clusters, overall utility of secondary network.

Based on **Algorithm 8** and **Algorithm 9**, each SU calculates $U_{SU}$ for respective PU offer.
Arranging the obtained $U_{SU}$ in descending order, each SU prepares preference list (PL) of PUs of length $|M|$.
PL of $N$ SUs is shared in the network and a preference matrix (PM) of size $[NXM]$ is constructed.
**Initialization:** $\pi = \phi$ ( There is no cluster in partition $\pi$).
**for** *k = 1 to —M—* **do**
  **for** *r = 1 to —N—* **do**
    **if** *(More than one ST have same PU preference)* **then**
      Identify available frames of preferred PU and rank the STs based on $U_{SU}$.
      **if** *(number of PU frames = = number of ranked STs)* **then**
        Group the ranked STs in $c_q$, include $c_q$ in $\pi$, map $c_q$ to the PU and assign each PU frame to the STs $\in c_q$.
        Mark the STs $\in c_q$ as assigned and the PU as completely mapped in PM.
        Calculate $GU_{c_q}$ by adding $U_{SU}$ of each ST $\in c_q$.
      **end**
      **if** *(number of PU frames < number of ranked STs)* **then**
        Identify top most STs equal to the number of PU frames and grouped them in cluster $c_q$ and include $c_q$ in $\pi$.
        **REPEAT** steps 10, 11, 12.
        Remaining STs wait for the next preferred PU in PM.
      **end**
    **else if** *(Each ST have individual PU preferences)* **then**
      **if** *(preferred PU is completely mapped)* **then**
        ST waits for its next preferred PU in PM.
      **else if** *(preferred PU is not completely mapped)* **then**
        Include ST to $c_q$, assign PU frame to ST and accordingly update $GU_{c_q}$ of $c_q$.
        Update status of the PU and mark it as completely mapped if remaining frame = 0
      **else if** *(preferred PU is not mapped yet)* **then**
        Form a new $c_q$, include $c_q$ in $\pi$ and **REPEAT** steps 23 and 24.
      **end**
    **end**
  **end**
  **if** *(N STs include in suitable clusters)* **then**
    Extract $\pi$ with all possible clusters formed.
    Calculate $OU_{SN}$ by adding $GU_{c_q}$ of each cluster included in $\pi$.
    Display the resultant clusters of $\pi$ and $OU_{SN}$ as the outcome of proposed $HG$.
    **STOP AND TERMINATE**.
  **else**
    **CONTINUE**
  **end**
**end**

with their preferred PU. This strategic pairing not only enhances the group utility of each cluster, denoted as $GU_{c_q}$, but also, in a concerted effort, maximizes the overall utility of the secondary network. The detailed steps of these cooperative techniques are comprehensively outlined in Algorithm 10, providing a systematic approach to achieving the desired clustering and PU mapping for optimized system performance.

**Time complexity of Algorithm 10:** Analyzing the time complexity of Algorithm 10 requires us to examine the running times of both the **For** loops, specifically those in steps 5 and 6. The outer **For** loop (step 5) iterates a maximum of $M$ times, as determined by the length of the PL, which corresponds to the total number of PUs. However, the time taken by the nested **For** loop (step 6) depends on two factors: the number of secondary users (SUs), denoted as $N$, and the number of transmission frames associated with each PU, allocated to the respective SUs. Let us assume, for instance, that $PT_1$ has $F_1$ frames, distributed among $F_1$ SUs out of the total $N$ SUs. Now, if $PT_2$ arrives with $F_2$ frames, these are assigned to the remaining SUs $(N - F_1)$. This process continues until we reach the last SU in the set of $N$, which corresponds to $(N - F_1 - F_2 - ...) = 1$. If we denote $F$ as the total number of frames in the network, in the worst-case scenario, this process repeats for $(N - F)$ times. Furthermore, in the worst-case scenario, where all SUs prefer the same PUs at each position in their preference list, the first **IF** condition in step 7 becomes true for each PU preference. Consequently, the process of ranking the secondary transmitters (STs) in step 8 is executed, which takes $log(M)$ time. As a result, the worst-case time complexity of Algorithm 10 can be expressed as follows: $O(M(N - F)log(M))$. Alternatively, we can simplify this to $O(MNlog(M))$. This time complexity falls within the category of polynomial time complexity, indicating that the algorithm is computationally efficient and manageable.

### 6.4.2 A Working Example

Let's illustrate the mechanism of Algorithm 10 with a practical example.

1. Consider a Cognitive Radio (CR) network comprising 5 primary users (PUs)

denoted as $PU_1, PU_2, PU_3, PU_4$, and $PU_5$, along with 8 secondary users (SUs), represented as $SU_1$ through $SU_8$. For simplicity, small number of frames for each PU is considered as depicted in Figure 6-10.

| $PU_1$ ($F_r = 2$) | $PU_2$ ($F_r = 3$) | $PU_3$ ($F_r = 2$) | $PU_4$ ($F_r = 4$) | $PU_5$ ($F_r = 5$) |
|---|---|---|---|---|

**Figure 6-10:** Considered PUs with associated frames

2. Each secondary transmitter ($ST$) computes its system utility $U_{SU}$, denoted as $U$ for brevity, with respect to each PU. These values are then arranged in descending order, creating a Preference List (PL) of PUs (as shown in Figure 6-11). The PL is then shared among all SUs.

| $SU_j =$ | $PU_4$ ($F_r = 2$) | $PU_5$ ($F_r = 5$) | $PU_3$ ($F_r = 2$) | $PU_1$ ($F_r = 2$) | $PU_2$ ($F_r = 3$) |
|---|---|---|---|---|---|

**Figure 6-11:** Preference List (PL) of PUs maintained by $SU_i$

3. Using their individual PLs, each SU constructs a Preference Matrix (PM) with dimensions $N \times M$, as shown in Figure 6-12.

| | 1st | 2nd | 3rd | 4th | 5th |
|---|---|---|---|---|---|
| $SU_1 =$ | **$PU_1$** (U = 5, $F_r$ =2) | **$PU_4$** (U = 4.5, $F_r$ =2) | **$PU_2$** (U = 4.2, $F_r$ =3) | **$PU_5$** (U = 4, $F_r$ =5) | **$PU_3$** (U = 3.9, $F_r$ =2) |
| $SU_2 =$ | **$PU_2$** (U = 5.2, $F_r$ =3) | **$PU_3$** (U = 5, $F_r$ =2) | **$PU_1$** (U = 4.3, $F_r$ =2) | **$PU_4$** (U = 4, $F_r$ =2) | **$PU_5$** (U = 3.7, $F_r$ =5) |
| $SU_3 =$ | **$PU_2$** (U = 4.8, $F_r$ =3) | **$PU_4$** (U = 4.6, $F_r$ =2) | **$PU_5$** (U = 4.3, $F_r$ =5) | **$PU_1$** (U = 4.1, $F_r$ =2) | **PU3** (U = 4, $F_r$ =2) |
| $SU_4 =$ | **$PU_1$** (U = 5.3, $F_r$ =2) | **$PU_5$** (U = 5, $F_r$ =5) | **$PU_4$** (U = 4.9, $F_r$ =2) | **$PU_2$** (U = 4.7, $F_r$ =3) | **$PU_3$** (U = 4.5, $F_r$ =2) |
| $SU_5 =$ | **$PU_3$** (U = 4.9, $F_r$ =2) | **$PU_1$** (U = 4.6, $F_r$ =2) | **$PU_2$** (U = 4.5, $F_r$ =3) | **$PU_5$** (U = 4.1, $F_r$ =5) | **$PU_4$** (U = 3.8, $F_r$ =2) |
| $SU_6 =$ | **$PU_4$** (U = 5.1, $F_r$ =2) | **$PU_1$** (U = 4.9, $F_r$ =2) | **$PU_2$** (U = 4.7, $F_r$ =3) | **$PU_5$** (U = 4.5, $F_r$ =5) | **$PU_3$** (U = 4.2, $F_r$ =2) |
| $SU_7 =$ | **$PU_1$** (U = 5.1, $F_r$ =2) | **$PU_5$** (U = 4.7, $F_r$ =5) | **$PU_2$** (U = 4.2, $F_r$ =3) | **$PU_4$** (U = 4, $F_r$ =2) | **$PU_3$** (U = 3.8, $F_r$ =2) |
| $SU_8 =$ | **$PU_2$** (U = 5.1, $F_r$ =3) | **$PU_4$** (U = 4.9, $F_r$ =2) | **$PU_5$** (U = 4.6, $F_r$ =5) | **$PU_3$** (U = 4.2, $F_r$ =2) | **$PU_3$** (U = 4, $F_r$ =2) |

**Figure 6-12:** Preference Matrix (PM) with dimensions $8 \times 5$

4. Examining $PM[1][1]$, we observe that $PU_1$ is the top preference for $SU_1$, $SU_4$, and $SU_7$. Since $PU_1$ has 2 available frames, and both $SU_4$ and $SU_7$ yield the highest $U$ values while paired with $PU_1$, they are grouped together to form Cluster $c_1$, which is mapped to $PU_1$. Subsequently, $SU_4$ and $SU_7$ are marked as "assigned", and $PU_1$ is marked as "completely mapped" in the PM. However, $SU_1$ is still waiting for its next preferred PU.

5. Similarly, $PU_2$ is the top preference for $SU_2$, $SU_3$, and $SU_8$. Given that $PU_2$ has 3 available frames, all three SUs ($SU_2$, $SU_3$, and $SU_8$) are grouped together to form Cluster $c_2$, which is mapped to $PU_2$. Consequently, $SU_2$, $SU_3$, and $SU_8$ are marked as "assigned", and $PU_2$ is marked as "completely mapped" in the $PM$.

6. However, $PU_3$ is the top preference of only $SU_5$. With $PU_3$ having 2 available frames, $SU_5$ forms Cluster $c_3$ by itself, mapped to $PU_3$. Subsequently, $SU_5$ is marked as "assigned", and $PU_3$ is marked as "partially mapped" in the $PM$.

7. Likewise, we find that $PU_4$ is the top preference for $SU_6$ alone. Since $PU_4$ has 2 available frames, $SU_6$ is placed in Cluster $c_4$, exclusively mapped to $PU_4$. In the Preference Matrix ($PM$), $SU_6$ is marked as "assigned", while $PU_4$ is labeled as "partially mapped".

8. So far, out of the 8 SUs ($N = 8$), 7 SUs ($SU_2$, $SU_3$, $SU_4$, $SU_5$, $SU_6$, $SU_7$, $SU_8$) have been successfully included in suitable clusters that are subsequently mapped to their preferred PUs. Only $SU_1$ remains unassigned, awaiting its next preferred PU, which is indicated in $PM[1][2]$.

9. Moving to $PM[1][2]$, we find that $PU_4$ is the second preference for $SU_1$. With one remaining frame available for $PU_4$, $SU_1$ is incorporated into the existing Cluster $c_4$, which is mapped to $PU_4$. Consequently, both $SU_6$ and $SU_1$ are now part of Cluster $c_4$. In $PM$, $SU_1$ is marked as "assigned", and $PU_4$ is denoted as "completely mapped".

This progression demonstrates how the cooperative clustering algorithm dynamically adapts to allocate SUs to their preferred PUs while efficiently utilizing available transmission frames.

Therefore, it is crucial to ensure that all SUs are grouped into clusters and that each cluster is paired with its preferred PU. The final mapping between these clusters and their preferred PUs is visually represented in Figure 6-13. In this mapping, we have established a total of four clusters ($|C| = 4$), adhering to the condition that the number of clusters ($|C|$) is less than or equal to the total number of available PUs ($|M|$). In cases involving clusters such as $c_3$ and $c_4$, the number of available frames for the associated PUs surpasses the count of cluster members. In such scenarios, specific cluster members are granted access to the surplus frames of their corresponding PUs. For instance, within cluster $c_3$, the

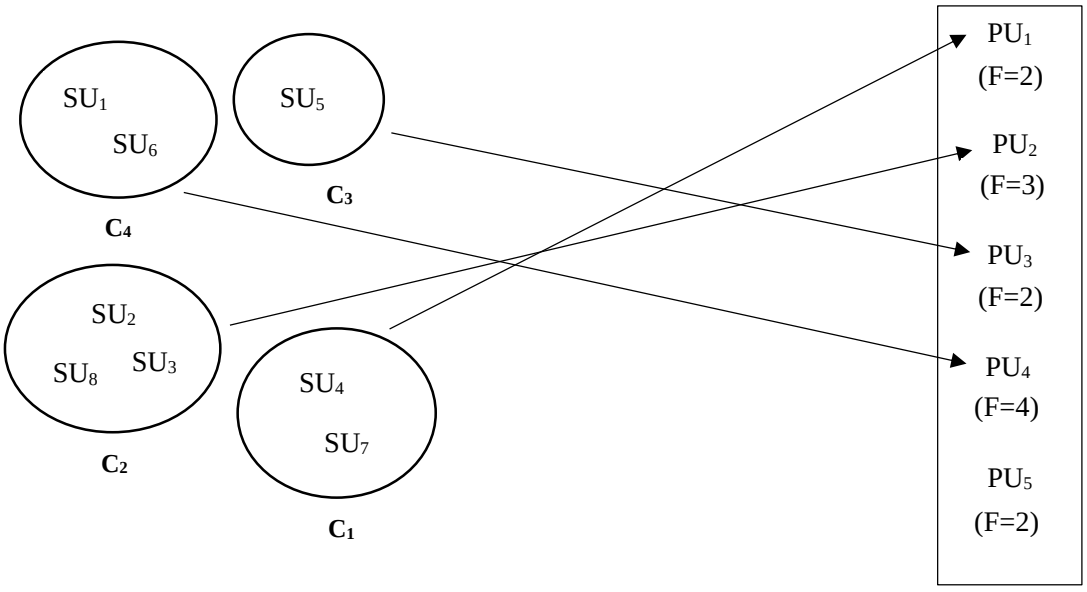


**Figure 6-13:** Final mapping among the cooperative SUs and preferred PU

cluster member $SU_5$ is granted permission to utilize the remaining frames allocated to $PU_3$. Similarly, within cluster $c_4$, the cluster members $SU_6$ and $SU_1$ are sequentially granted access to the surplus frames of $PU_4$. This allocation strategy optimally utilizes available resources while ensuring efficient cooperation among SUs and PUs. It's important to highlight that, after completing the final mapping of each cluster to its designated PU, if there are any frames of the mapped PU that remain unallocated, the higher-ranked STs within their respective clusters are given access to these remaining PU frames in a sequential fashion. Furthermore, in the final mapping shown in Figure 6-13, we can notice that $P_5$ is not assigned to any of the four clusters. This observation suggests that, in the worst-case scenario where a higher number of STs primarily prefer the same PTs, the less preferred PTs may go unmapped within the proposed cooperative communication framework. Addressing this issue could involve exploring the concept of many-to-many mapping between the set of PUs and SUs. However, it is worth noting that this area requires further investigation and development to fully resolve such concerns.

### 6.4.3 Theoretical analysis of Algorithm 3 based on Hedonic Game concept

***Theorem 1***: The partition $\pi = \sum_{q=1}^{|C|} c_q$ obtained by applying Algorithm 10 is Individually Rational.

***Proof***: Algorithm 10 partitions the set of $N$ SUs into $C$ clusters, ensuring that each SU becomes a member of a favorable cluster $c_q$ mapped to its

preferred PU. This arrangement fosters cooperative communication between each SU within $c_q$ and its preferred PU, resulting in an increase in both the individual system utility ($U_{SU}$) of the SUs and the group utility of $c_q$. In the proposed Hedonic coalition formation game (HG), there exists no incentive for any SU to pursue an individual strategy. Instead, every SU acknowledges the benefits of cooperative participation, willingly becoming a member of a suitable cluster that collectively accesses the preferred PU spectrum for cooperative communication. Thus, it is established that the partition $\pi = \sum_{q=1}^{|C|} c_q$ derived from Algorithm 10 conforms to the principle of being Individually Rational.

***Theorem 2***: The partition $\pi = \sum_{q=1}^{|C|} c_q$ obtained by applying Algorithm 103 is Nash Stable.

***Proof***: Algorithm 10 is designed to create $C$ clusters, each comprising one or more SUs as cluster members. Importantly, this construction ensures that, by being part of their designated cluster, denoted as $c_q$, each SU can be effectively paired with their preferred PU for cooperative communication. This strategic arrangement significantly enhances the likelihood that every SU within $c_q$ will achieve the highest attainable $U_{SU}$, consequently maximizing the group utility of cluster $c_q$. Given this setup, each SU belonging to $c_q$ exhibits a strong preference for remaining within that same cluster. The reason is straightforward: migrating to a different cluster would disrupt the mapping with their preferred PU, resulting in a decrease in the $U_{SU}$ for each SU. Therefore, any unilateral deviation by an SU from their current cluster to a new one does not offer any advantage to any of the SUs, and such deviations are not observed in this context. As a result, we have successfully demonstrated that the partition $\pi$ of the set of $N$ SUs into $C$ clusters, as obtained through Algorithm 10, adheres to the principle of Nash Stability.

***Theorem 3***: The partition $\pi = \sum_{q=1}^{|C|} c_q$ obtained by applying Algorithm 10 is Core Stable.

***Proof***: Building upon the earlier proof of Nash Stability, we can confidently assert that Algorithm 10 prohibits any unilateral deviation by the SUs from their current cluster to a new one. In essence, each SU strongly prefers their existing cluster over all other clusters within the partition $\pi$. This preference is grounded in the substantial advantages conferred upon each SU by remaining a member of their current cluster. As a direct consequence of this preference alignment, there is no possibility of forming any blocking clusters by any of the SUs within $\pi$. This underscores the notion that the partition $\pi$ of the set of $N$ SUs into $C$ clusters, as facilitated by Algorithm 10, fully aligns with the concept of

Core Stability.

## 6.5 Numerical Results and Comparison Analysis

The performance assessment of our proposed energy harvesting, power allocation, and cooperative communication strategies, in comparison to both optimal (benchmark result obtained from lingo optimization tool) and existing schemes, is conducted through a simulation-based study using MATLAB 7 (R2017a). The simulation runs on a 64-bit PC equipped with a core i5 processor and 8 GB RAM. Our simulation focuses on a Cognitive Radio (CR) network, featuring $M$ primary users (PUs) and $N$ secondary users (SUs), where $M$ is less than $N$. The spatial distribution of PUs and SUs is random, spanning a square area measuring $1000 \times 1000\ m^2$. Specifically, the PU transceiver pairs are positioned at an average distance of approximately 30 $m$ from each other, while the SU transceiver pairs are, on average, 20 $m$ apart. Furthermore, the specific simulation parameters and their corresponding values are listed in Table 6.3. These meticulously chosen parameters and settings form the foundation for our comprehensive evaluation of the proposed solutions within the context of the CR network under investigation.

| Parameters | Values |
|---|---|
| M | 5 to 20 |
| N | 5 to 50 |
| F | 5 to 10 (variable) |
| $T_1 = T_2 = T_3$ | 10 sec |
| W | 1 MHz |
| $P_{PT}$ | 1 Watt |
| $E_{ST}^{max}$ | 35 Joule |
| $BE_{finite}$ | 40 Joule |
| $R_{PT}^{tar}$ | 5 to 7 bps (variable) |
| $R_{ST}^{tar}$ | 3 to 6 bps (variable) |
| $d_{u,v}$ | 30 to 20 m (variable) |
| $\sigma^2_{N_{0,a}} = \sigma^2_{N_{0,cov}}$ | 1 mW |
| $P_{ST}^{min}$ | 20 to 30 mW |
| path loss exponent | 2 |

Table 6.3: Simulation parameters and their values

To assess the effectiveness of our proposed cooperative communication model, we examine a CRN scenario with an increasing number of SUs, $N$ ranging from 10 to 50, while keeping the number of PUs, $M$ fixed at different values (namely, 5, 10, 15, and 20). In this scenario, each PU is equipped with a vari-

able number of transmission frames, ranging from 5 to 10 frames. Additionally, to provide a basis for comparison, we also consider an energy harvesting Non-Cooperation (NC) scenario involving interactions among PUs and SUs. In this NC approach, each SU engages in competitive interactions with other SUs to establish a connection with their preferred PU, with the goal of participating in cooperative communication. On the flip side, PUs evaluate offers from SUs to identify the most advantageous SU for optimizing their primary utility. This process leads to the establishment of one-to-one mappings between PUs and SUs, illustrating the dynamics of non-cooperative behavior in contrast to our proposed cooperative communication model.

### 6.5.1 Performance Metrics

Following metrics have been used for simulation based performance analysis.

- $\alpha^*, \rho^*$: The optimal time switching factor and power splitting factor for energy harvesting by SU that are calculated based on Eq. (6.17).
- $EH_{T_1}^{prop}$: Energy harvesting by SUs during Phase 1 that calculate based on Eq. (6.6).
- $R_{T_1}^{prop}$: Decoding rate obtained by SUs during Phase 1 that calculate based on Eq. (6.7).
- $x^*$, $y^*$: The optimal power allocation factors for SUs during Phase 2 and 3 that calculate based on Eq. (6.18).
- $HP_{ST}^{prop}$: Power harvested by SUs after Phase 1 that calculate based on Eq. (6.8).
- Average utility of PUs (avg. $U_{PU}$): Utility achieved by $M$ number of PUs that calculate based on Eq. (6.30).
- Average utility of SUs (avg. $U_{SU}$): Utility achieved by $N$ number of SUs that calculate based on Eq. (6.16).
- Average satisfaction of SUs (avg. $SAT_{ST}$): Satisfaction achieved by $N$ number of SUs that calculate based on Eq. (6.27).
- Percentage of participation of SUs ($\%P_{ST}$): Out of total 100 number of SUs, how many SUs can able to participated in the cooperative communication with PU that calculate based on Eq. (6.29).

### 6.5.2 Utility of SUs in proposed cooperation scheme vs. non-cooperation scheme

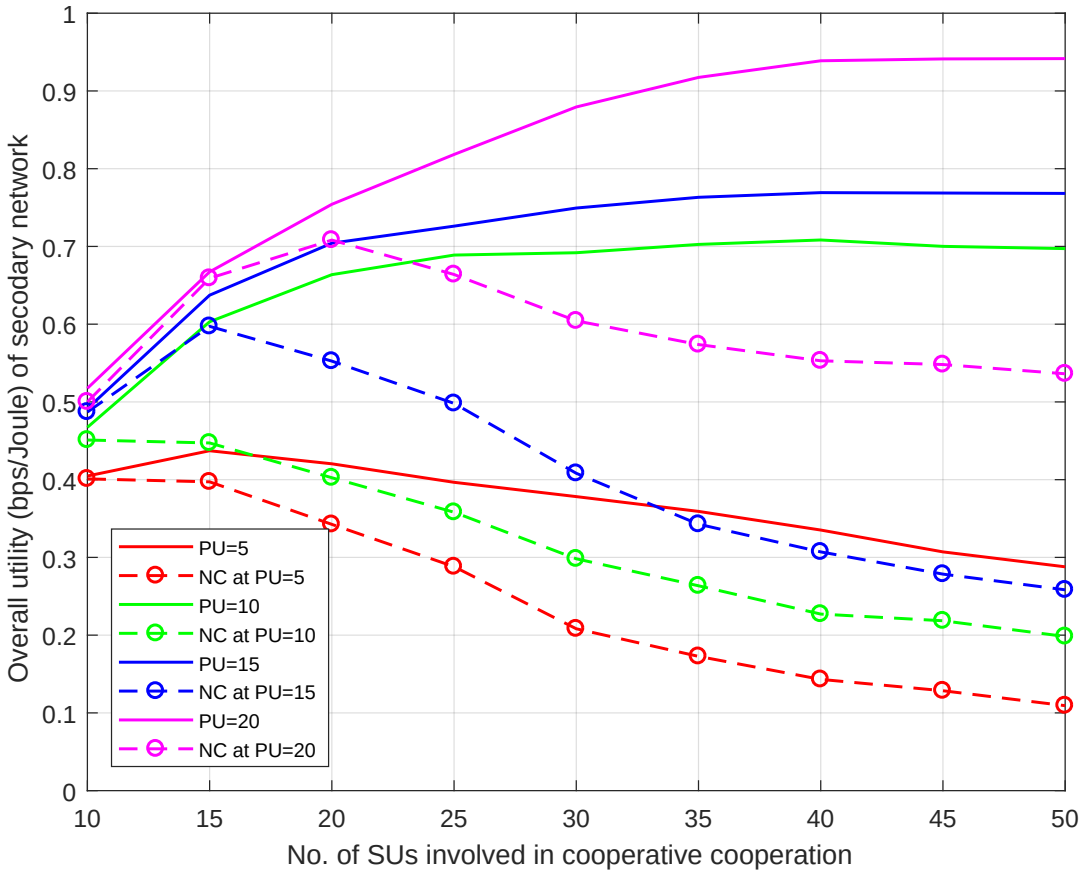


**Figure 6-14:** Overall utility of secondary network vs. varying no. of PUs and SUs in cooperation process

Figure 6-14 depicts the overall utility of the secondary network ($OU_{SN}$), with increasing number of SUs while maintaining a fixed number of PUs. In the case where $M = 5$ (indicated by the red line), $OU_{SN}$ experiences a decline with the growing number of SUs in the network. This decline can be attributed to two key factors: (i) the available PU frames become insufficient to accommodate the increasing number of SUs or (ii) SUs may end up being paired with less preferred PUs due to limited PU preferences. However, when more PUs are introduced into the network, the number of PU preferences and consequently the number of available PU frames increase. This, in turn, enhances the likelihood of SUs being assigned to clusters that align with their preferred PUs. As a result, there is a significant improvement observed in the System Utility ($U_{SU}$) of each SU, the group utility of each cluster, and ultimately the $OU_{SN}$ of the secondary network (as indicated by the green, blue, and purple solid lines, respectively).

In contrast, when considering the Non-Cooperation (NC) approach, the initial observation reveals an upward trend in the overall utility of SUs. However, this trend abruptly shifts towards deterioration once a certain threshold of SUs in the network is surpassed. The decline in utility can be attributed to the increasing availability of new SU options within the network. This abundance of choices empowers PUs to selectively pair with the most suitable SUs while potentially rejecting previously established mappings. As a consequence, this rejection process significantly diminishes the attainable utility of the secondary network, as evident in the graph (illustrated by the four dotted lines).

### 6.5.3 Satisfaction of SUs in proposed cooperation scheme vs. non-cooperation scheme

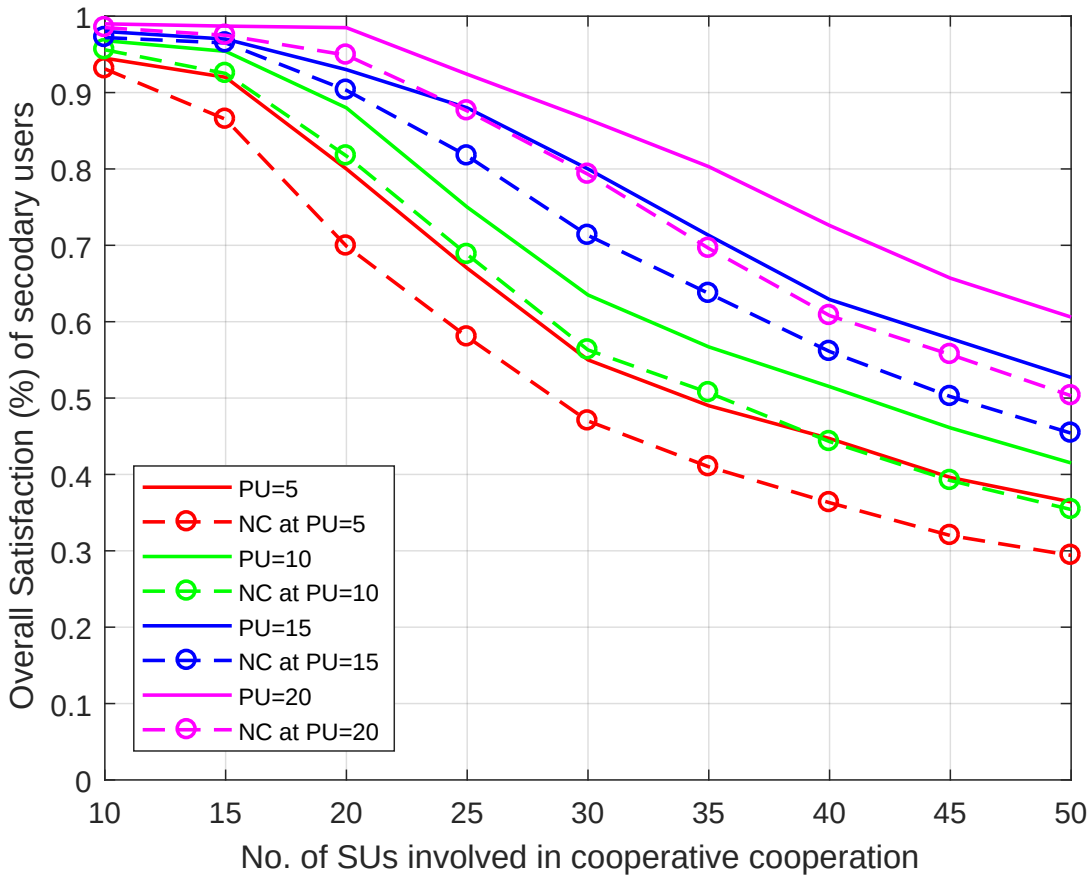


**Figure 6-15:** Overall satisfaction of SUs vs. varying no. of PUs and SUs in the cooperative process

Next, let us analyze the overall satisfaction of each involved SU ($SAT_{ST}$) within the proposed cooperative communication, as illustrated in Figure 6-15. Taking inspiration from [94], the $SAT_{ST}$ of $N$ SUs in case of a non-cooperative

approach ($SAT_{ST}^{NC}$) is formulated as follows:

$$SAT_{ST}^{NC} = \frac{\sum_{j=1}^{N}(M+1) - p_j}{MN} \tag{6.26}$$

Here, $M$ represents the total number of PUs, and $p$ denotes the position of a PU in the preference list of an SU. The concept of Eq. 6.26 can be adapted to reformulate the satisfaction of SUs for the proposed cooperative approach within a scenario involving a total of $C$ clusters and $v$ instances of stable $PT-ST$ mapping ($S_{PT,ST}$) within each cluster, as follows:

$$SAT_{ST} = \frac{\sum_{1}^{|C|}\left(\sum_{j=1}^{|v|}(S_{PT,ST}+1) - p_j\right)}{\sum_{1}^{|C|}\left(\sum_{1}^{|v|} S_{PT,ST}\right) N} \tag{6.27}$$

Based on the formula mentioned above, we illustrate the $SAT_{ST}$ achieved by the proposed cooperative model in Figure 6-15. Initially, it is evident that the overall satisfaction of all SUs, across different $M$ values, is notably high (above 90%). However, as the number of SUs in the network increases, the $SAT_{ST}$ graphs for all four cases of PUs begin to decline after reaching certain thresholds (represented by the solid lines). This decrease is attributed to a limited number of suitable PU options available in the network compared to the growing number of SUs, which results in fewer SUs being able to establish mappings with their preferred PUs. Consequently, the value of $p$ for each $S_{PT,ST}$ mapping within a cluster decreases, ultimately leading to a decrease in $SAT_{ST}$.

When comparing the $SAT_{ST}$ achieved through the proposed method with the $NC$ approach, as discussed in [94], it becomes apparent that the proposed method outperforms the $NC$ approach, as depicted in Figure 6-15 (represented by the dotted lines). This superiority arises from the repeated rejections faced by SUs in the $NC$ approach, which either forces SUs to pair with their least preferred PUs or results in their exclusion from the cooperative process, leading to a reduction in SUs' satisfaction levels.

### 6.5.4 Participation of SUs in proposed cooperation scheme vs. non-cooperation scheme

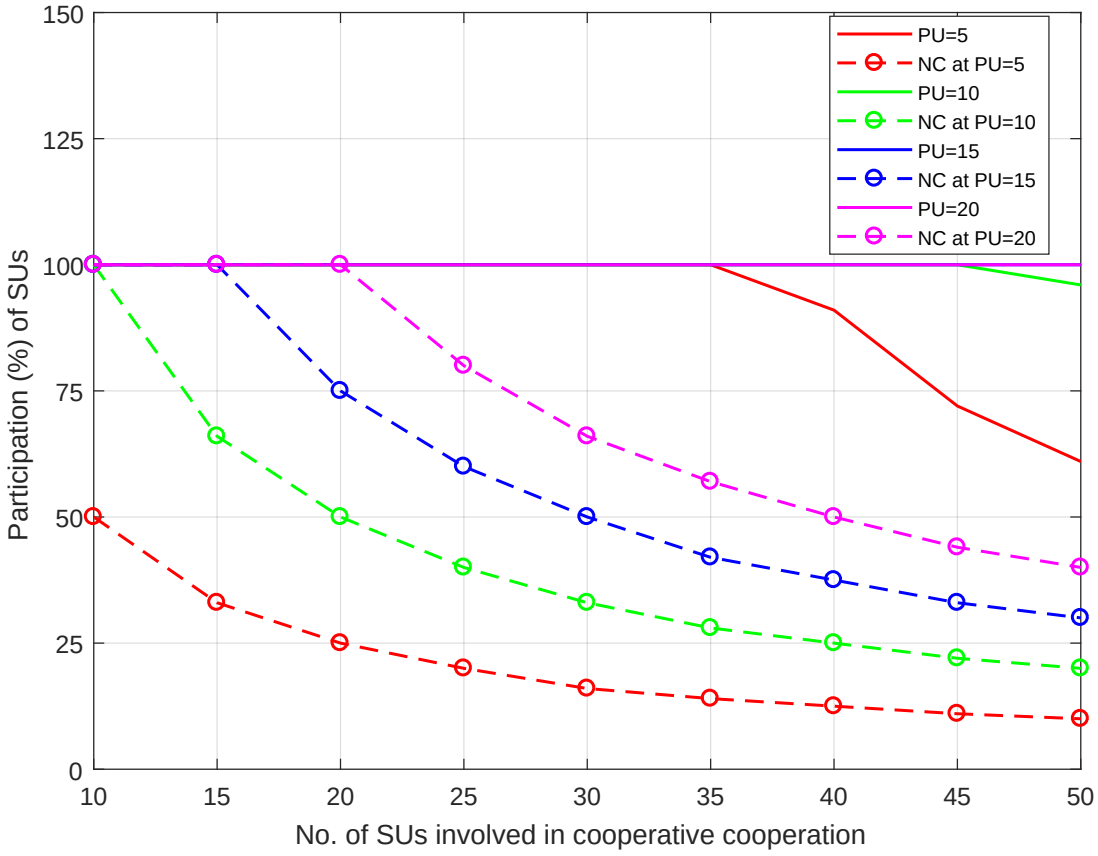


**Figure 6-16:** Participation of SUs vs. varying no. of PUs and SUs in the cooperative process

To further investigate the engagement of SUs in cooperative communication, we analyze the percentage of SUs participating ($\%P_{ST}$) and compare its performance with the $NC$ approach, as illustrated in Fig. 6-16. In the case of the $NC$ approach, the $\%P_{ST}$ is computed as follows:

$$\%P_{ST}^{NC} = \frac{\text{Number of SUs involve in coop. communication}}{\text{Total number SUs}} \times 100\% \qquad (6.28)$$

However, for the proposed cooperative approach, we modify the above formula as follows:

$$\%P_{ST} = \frac{\sum_{1}^{|C|} (\text{Number of SUs in each cluster})}{\text{Total number SUs}} \times 100\% \qquad (6.29)$$

In Figure 6-16, we can observe that when there are 20 and 15 PUs in the network (represented by the purple and blue solid lines), all 50 SUs (100% of them) are able to participate in the proposed cooperative process. However, as the number

of SUs in the network increases further, we notice a slight reduction in $\%P_{ST}$ for $M = 10$ and a relatively larger reduction for $M = 5$ (shown in the green and red solid lines). This reduction occurs because the limited number of available PUs in the network can only accommodate SUs that offer significant cooperative benefits.

In contrast, when considering the $NC$ approach, full participation of SUs is achieved for all four values of $M$, but only up to the point where $M$ is equal to $N$ in the network. This limitation arises from the one-to-one mapping employed in the $NC$ technique, where only SUs with an equal number of PUs can participate in cooperative communication. The graph illustrates a noticeable decrease in $\%P_{ST}^{NC}$, as shown by the dotted lines.

### 6.5.5 Utility of PUs with varying size of networks

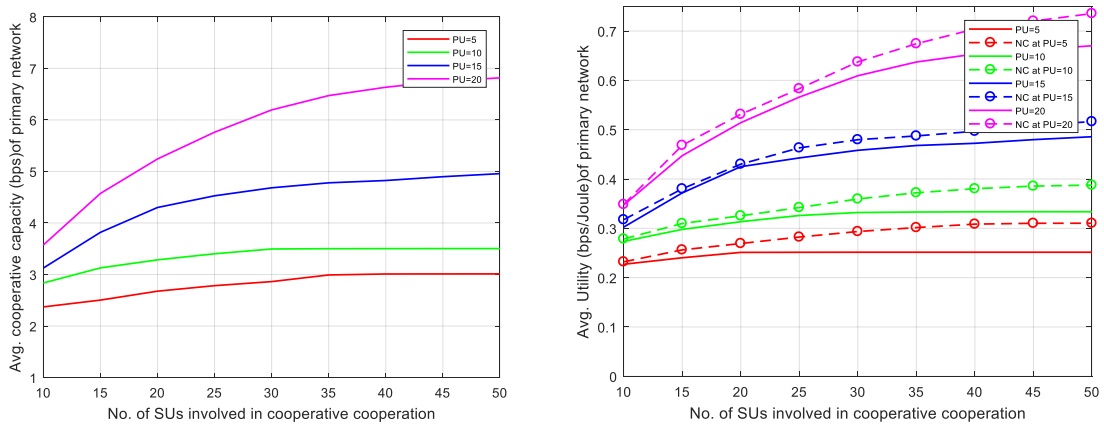


**Figure 6-17:** (a) Average cooperative capacity of PU (b) Average utility of PUs for varying no. of PUs and SUs

At last, we assess the effectiveness of the primary network in the proposed cooperative communication approach by examining the cooperative capacity achieved by PU ($C_{PT}^{coop}$ (as defined in Eq. (6.13))) and utility of PUs. The formulation of utility function of each PU is modeled in terms of the achieved $C_{PT}^{coop}$ assisting with suitable ST, per unit energy consumption rate of the PT during $T_1$ time ($EC_{PT} = P_{PT} \times T_1$). Thus, the average utility of the primary network ($U_{PU}$) for $M$ PUs in the network is calculated as follows:

$$U_{PU} = \sum_{i=1}^{|M|} \frac{C_{PT_i}^{coop}}{EC_{PT_i}} \tag{6.30}$$

In Figure 6-17 (a) and (b), the graphs of average $C_{PT}^{coop}$ and avg. $U_{PU}$ are depicted respectively. In Figure 6-17 (a), it is evident that for various values of $M$, the average $C_{PT}^{coop}$ gradually rises with an increase in the number of SUs in the network. This occurs from the fact that, with the growth in the number of SUs, the count of cooperative SUs within each cluster also increases. This maximizes the access to each frame of PU bands, consequently enhance the $C_{PT}^{coop}$ for each PU. However, in case of $M = 5$ and $M = 10$, the $C_{PT}^{coop}$ reaches a saturation point (red and green lines) despite an increase in the number of SUs participating in the cooperation model. This saturation occurs because the relatively smaller number of PUs and their associated frames cannot accommodate the growing number of SUs for cooperative communication. It is noted that $C_{PT}^{coop}$ is achieved exclusively through cooperation between PUs and SUs, so there is no point of comparison with non-cooperative methods in this case.

Similar effect for scenarios with $M = 5$ and $M = 10$ PUs (red and green solid lines) is observed in Figure 6-17 (b), where avg. $U_{PU}$ saturates even as the number of SUs continues to increase. However, a gradual increase in avg. $U_{PU}$ is evident in the graph for the cases of $M = 15$ and $M = 20$ PUs (blue and purple solid lines). This increase is attributed to the larger number of SUs that can successfully group in suitable clusters and get mapped with suitable PUs for cooperative communication, resulting in a significant improvement in both the utility of SUs and avg. $U_{PU}$ for the primary network.

In contrast, the $NC$ strategy outperforms the proposed cooperative technique by achieving the highest attainable avg. $U_{PU}$ for various values of $M$ PUs. In the $NC$ strategy, as the number of SUs in the network increases, each PU receives a greater number of SU requests. This increased availability of SUs enables PUs to improve their selection of suitable SUs as cooperative partners by rejecting their initial choices. As a result, the graph illustrates a significant increase in avg. $U_{PU}$ for all $M$ values, as indicated by the four dotted lines.

## 6.6 Conclusion

In this chapter, we proposed an energy-harvesting technique tailored for energy-constrained Cognitive Radio Networks engaged in cooperative communication with primary users (PUs). Our investigation focused on two optimization objectives: maximizing harvested energy at secondary users (SUs) by optimizing time-switching and power-splitting factors, and maximizing the system utility of

SUs through optimal power allocation. We developed two sub-optimal solutions for these problems, achieving 97.7% and 98.5% accuracy respectively when compared against optimal results. To enhance the individual and collective utility of SUs, we proposed a cooperative communication framework based on a hedonic cluster formation game. In this framework, SUs autonomously form clusters to seek favorable PU partnerships for cooperative communication. We provided formal proofs supporting the effectiveness of this hedonic game-based cooperative model. Our results demonstrated that the proposed cooperative model outperforms the non-cooperative approach in terms of overall SU utility, SU satisfaction, and SU participation during cooperation.